universität wien

MASTERARBEIT | MASTER'S THESIS

Titel | Title

Anticancer Potential of Ferrocene-Modified Tridentate Naphthoquinone-Based Organometallics

verfasst von | submitted by

Robin Pfister BSc

angestrebter akademischer Grad | in partial fulfilment of the requirements for the degree of

Master of Science (MSc)

Wien | Vienna, 2026

Studienkennzahl lt. Studienblatt | Degree programme code as it appears on the student record sheet:	UA 066 862
Studienrichtung lt. Studienblatt | Degree programme as it appears on the student record sheet:	Masterstudium Chemie
Betreut von | Supervisor:	Assoz. Prof. Mag. Dr. Christian Kowol
Mitbetreut von | Co-Supervisor:	Dipl.-Ing. Dr. Wolfgang Kandioller

Acknowledgements

This thesis is not a palace made of jasper, but a foundation built from rocks and bricks and gravel. I want to thank all those who's support made this work possible. Thank you for handing me the stones that make up the ground beneath my feet.

I would like to thank Prof. Christian Kowol, Dr. Wolfgang Kandioller, and Dr. Michael Jakupec for their supervision and guidance. The synthetic work I conducted was pure joy also because of the kind and supportive colleagues in and around lab 6. Special thanks goes to Alex and Paul for handing down their knowledge and experience in a warm-hearted way, as well as to Claudia, Judith, and Joni for fun times and good laughs. I am equally indebted to the people of the cell culture facility for their welcoming and patient way of introducing me to a new environment. Thank you Dominik, Slavica, Michaela, and Dina!

During the last seven years in Vienna I was very fortunate to make a lot of new acquaintances and friends. I would like to thank all of them and to express my special gratitude to those who have been by my side since the early days of my studies, namely to Kathi, Vera, Rebecca, and Isa of the Double Chocolate Chip Cookies!

When the western winds carried me to Vienna I did not come alone. To my friends who joined me but also to those who remained in Vorarlberg: thank you for your friendship which overcomes even the greatest distances! Last but not least I would like to thank my family. They have known me the longest and they love me anyway. Thank you for your enduring support!

Thank you everyone for being part of my path. You make this foundation of rocks and bricks and gravel the most wonderful mosaic.

Abstract

Cancer is a group of diseases with tremendous impact on society, responsible for millions of premature deaths. In order to tackle this burden, various therapeutic approaches have been established, with chemotherapy being one of them. As approved anticancer agents are by no means universally applicable for all patients or types of cancer and are often associated with adverse effects, research on novel tumor-inhibiting agents remains indispensable. Since the discovery of cisplatin and its anti-proliferative properties, metal-based anticancer agents have emerged as a promising group of chemotherapeutics. More recent research extended its focus on complexes of transition metals such as ruthenium, iridium, and osmium, resulting in compounds showing tumor-inhibiting potential in preclinical and clinical studies. A group of naphthoquinone-based ruthenium complexes showed particularly high cytotoxicity when tested on SW480 cells. The mode of action exhibited by these organometallics has yet to be fully illuminated, but first insights suggest that no reactive oxygen species (ROS) are generated in tested cells. Incorporation of ROS-inducing groups may increase the cytotoxicity of naphthoquinone-based ruthenium and osmium organometallics even further, making them a reasonable starting point for additional investigations. Ferrocene moieties could potentially be used as ROS-inducing groups, as ferrocene is known to participate in reactions leading to ROS formation.

In this thesis, ferrocene-modified osmium organometallics were synthesized and characterized using NMR-spectroscopy, mass spectrometry (MS), elemental analysis, single crystal X-ray diffraction, and UV–vis spectroscopy. Alongside their ruthenium analogs and free ligands, the synthesized complexes were tested for their biological behavior *in vitro*. Their cytotoxicity, ROS inducing capabilities, and cellular accumulation were assessed using MTT tests, DCFH-DA assays, and inductively coupled plasma-MS, respectively.

Several tested compounds exhibited pronounced cell growth inhibition with IC_{50} values in the nanomolar range, which correlated with their enhanced cellular accumulation. None of the tested complexes induced significant levels of ROS, but a ferrocene-modified naphthoquinone ligand lead to ROS levels exceeding those of the negative control, indicating that the introduction of a ferrocene moiety can indeed lead to ROS induction. Further investigations are necessary to evaluate the implementation of ferrocene as a ROS-inducing group into the tested class of organometallics.

Zusammenfassung

Krebs ist eine Gruppe von Krankheiten mit immensen gesellschaftlichen Auswirkungen und ist verantwortlich für Millionen von frühzeitigen Todesfällen. Verschiedene Ansätze existieren, um diesem Leidensdruck entgegenzuwirken, wie beispielsweise die Chemotherapie. Chemotherapeutika sind keineswegs universell einsetzbar und haben häufig unerwünschte Nebenwirkungen, weshalb Forschung an neuen Medikamenten unerlässlich bleibt. Seit der Entdeckung von Cisplatin und seiner tumorinhibierenden Wirkung haben sich metallbasierte Krebstherapeutika zu einem wichtigen Forschungsfeld entwickelt. Komplexe weiterer Übergansmetalle, wie beispielsweise Ruthenium, Iridium und Osmium, rücken zunehmend in den Fokus und haben zahlreiche Komplexverbindungen mit tumorinhibierender Wirkung hervorgebracht. Eine Gruppe naphthochinonbasierter Rutheniumkomplexe zeigte besonders ausgeprägte Zytotoxizität in Tests mit SW480 Zellen. Der Wirkmechanismus bedarf weiterer Aufklärung, doch erste Ergebnisse zeigen, dass in behandelten Zellen keine reaktiven Sauerstoffspezies (ROS) entstehen. Das Implementieren ROS-generierender Gruppen in naphthochinonbasierte Ruthenium- und Osmiumkomplexe könnte deren Zytotoxizität zusätzlich steigern, weshalb sie einen möglichen Ausgangspunkt für weiter Nachforschungen darstellen. Ferrocen könnte als eine solche Gruppe agieren, da es sich an Reaktionen beteiligt, die ROS erzeugen.

Im Rahmen dieser Arbeit wurden ferrocen-modifizierte organometallische Osmiumkomplexe synthetisiert und mittels NMR-Spektroskopie, Massenspektrometrie (MS), Elementaranalyse, Einkristalldiffraktometrie und UV–vis Spektroskopie charakterisiert. Biologische Interaktionen der Osmiumkomplexe, ihrer Rutheniumanaloga und der freien Liganden wurden *in vitro* untersucht. Die Zytotoxizität, das Vermögen ROS zu induzieren, sowie die Akkumulation in Zellen wurden mittels MTT-Tests, DCFH-DA-Assays und induktiv gekoppelter Plasma-MS ermittelt.

Mehrere getestete Verbindungen inhibierten das Wachstum von Krebszellen mit IC_{50}-Werten im nanomolaren Bereich, wobei keiner der getesteten Komplexe zu signifikanter ROS-Induktion führte. Ein ferrocen-modifizierter Naphthochinon-Ligand erhöhte jedoch die ROS-Konzentration signifikant, was darauf hindeutet, dass Ferrocen als ROS-induzierende Gruppe verwendbar ist. Weitere Nachforschungen sind notwendig um die Verwendung von Ferrocen als ROS-induzierende in der getesteten Substanzklasse zu beurteilen.

Table of Contents

List of Figures

List of Tables

List of Abbreviations

5-FU 5-fluorouracil

COSY ..... correlation spectroscopy

CQ ..... chloroquine

DCF ..... 2',7'-dichlorofluorescein

DCFH-DA ..... 2',7'-dichlorodihydrofluorescein diacetate

DCM ..... dichlormethane

DMEM/F12 ..... Dulbecco's Modified Eagle's Medium/Nutrient Mixture F-12 Ham

DMSO ..... dimethyl sulfoxide

DNA ..... deoxyribonucleic acid

EDTA ..... ethylenediaminetetraacetic acid

EMEM ..... Minimum Essential Medium Eagle

eq ..... equivalent

ER ..... endoplasmatic reticulum

ERα^+ ..... estrogen receptor α -positive

EtOAc ..... ethyl acetate

FBS ..... fetal bovine serum

Fc ..... ferrocene

FQ ..... ferroquine

HBSS ..... Hanks' Balanced Salt Solution

HDI ..... human development index

HMBC ..... heteronuclear multiple bond coherence

HNO_3 ..... nitric acid

HSQC ..... heteronuclear single quantum coherence

IC_{50} ..... concentration at which cell growth is inhibited by 50%

ICP ..... inductively coupled plasma

LC ..... liquid chromatography

MeOH ..... methanol

MPLC ..... medium pressure liquid chromatography

MS ..... mass spectrometry

MTT . . . . . 3-(4,5-dimethylthiazol-2-yl)-2,5-diphenyl-2H-tetrazolium bromide

NEt_3 . . . . . triethylamine

NH_3 . . . . . ammonia

nHex . . . . . n-hexane

NMR . . . . . nuclear magnetic resonance

OD . . . . . optical density

OptiMEM . . . . . phenol red free OptiMEM®

PBS . . . . . Dulbecco's Phosphate Buffered Saline

PEG . . . . . polyethylene glycol

RNA . . . . . ribonucleic acid

r.t. . . . . . room temperature

ROS . . . . . reactive oxygen species

RPMI 1640 . . . . . Roswell Park Memorial Institute 1640 medium

SXRD . . . . . single crystal X-ray diffraction

TAM . . . . . tamoxifen

TBHP . . . . . tert-butyl hydroperoxide

Software and Tools

Function	Tool
Text Editor	Texmaker 5.0.4
Chemical Structures	ChemDraw 21.0.0.28
NMR Analysis	MestReNova 14.1.2-25024
X-Ray Structures	Olex2 1.5
Citation Software	Zotero 7.0.32
Graphing	OriginPro 2025b 10.2.5.234
Research	Google Scholar
	ChatGPT March5

1 Introduction

Cancer is a group of diseases with enormous impact on society. As one of the leading causes for premature death it constitutes a huge burden on human health, with future projections indicating increases in incidences, which give reason for concern. To tackle this burden, great effort is put into cancer research, developing novel drugs and designing therapeutic strategies. Chemotherapy development is a prolific field of research and has brought forth numerous clinically approved anticancer drugs, with platinum complexes being one of the indispensable classes of chemotherapeutic agents. Coordination compounds containing ruthenium and osmium have already shown promising results in preclinical cancer research, although they are yet to be clinically approved. While the synthesis of novel compounds is essential in this field, preclinical evaluation is crucial to determine their potential as anticancer agents and to pave the way for clinical investigation. With the establishment of cell culture techniques, cancer research gained a versatile instrument for preclinical evaluation of drug candidates. By cultivating cancer cells *in vitro,* numerous assays can be performed without compromising human or animal health. For this thesis, various assays were performed on cultivated cancer cells to characterize biological interactions of the tested Ru and Os complexes.

1.1 Cancer

Cancer has been known to humanity for thousands of years. The abnormal growth of cancerous ulcers has already been described in times of old Egypt,[1] while the word 'cancer'—originating from the Greek word karkinos (*καρκινος*)—has its origin in ancient Greece.[2] With today's knowledge, cancer can be defined as a group of diseases, which lead to uncontrolled cell proliferation.[3] The global cancer burden is tremendous, although cancer arises from a series of minor alterations to normal cells, summarized as the hallmarks of cancer.

1.1.1 Origin and Progression

Normal cells progress through a series of stages collectively known as the cell cycle, during which they grow, replicate their deoxyribonucleic acid (DNA), and divide into two daughter cells. This process is tightly regulated by internal and external signals, which coordinate gene expression and control cell proliferation. Deregulation of the cell cycle is a cancer hallmark. By altering gene transcription and inactivating tumor suppressor genes, cancer cells bypass normal regulatory mechanisms and evade programmed cell death known as apoptosis.

1.1.2 Hallmarks of Cancer

The complex multi-step mechanism of cancer development and progression—the knowledge of which is still far from complete—can be structured into several participating key factors. These so-called 'Hallmarks of Cancer' are subject to continuous additions, incorporating most recent findings in cancer research. The following paragraphs summarize hallmarks and emerging hallmarks postulated by Hanahan and Weinberg.[4–6]

Sustaining Proliferative Signalling. Proliferation of normal cells is strictly regulated by growth-promoting signals. By deregulating these signals, cancer cells can acquire the ability to sustain mitotic activity beyond normal extent. This may be achieved by production of new growth factors, increasing the number of growth factor receptors, or stimulating surrounding normal cells to deliver growth factors.

Evading Growth Suppressors. The number of cells in normal tissue is also regulated by growth suppressors. Growth-suppressing systems are a powerful barrier to abnormal proliferation, which many types of cancer need to overcome to enable uncontrolled growth. This is often achieved by interference with tumor suppressor genes such as *TP53* or *RB1*.

Avoiding Immune Destruction. The immune system is essential for human survival. It effectively detects and eradicates pathogens and abnormal cells, making it another important obstacle to the emergence of cancer. Avoiding detection by the immune system enables cancer cells to proliferate undisturbed, leading to tumor progression.

Enabling Replicative Immortality. Normal cells can only undergo a limited number of divisions before they enter the senescent phase, followed by programmed cell death. Replicative senescence and apoptosis, therefore, constitute a natural limitation to cell proliferation, contributing to homeostasis. By escaping this natural cycle, cancer cells attain replicative immortality. One way of achieving potentially unlimited proliferation is by enhancing telomerase activity, hindering the natural shortening of telomeres and thus avoiding entrance into crisis and apoptosis.

Tumor-Promoting Inflammation. Inflammation is an immune response to tissue damage or infection and is frequently observed in cancerous tissues. Although it normally serves a protective function, chronic inflammation can contribute to tumor development and progression. Inflammatory signals from the tumor microenvironment can

promote cell proliferation and survival. In addition, inflammatory processes often lead to the production of reactive oxygen species (ROS), which can cause further genomic damage.

Activating Invasion & Metastasis. A typical characteristic of malignant tumors is the invasion into surrounding tissue and the formation of metastases. While normal cells are growing in association with neighbouring cells, cancer cells can escape from this bond and migrate into normal tissue, enabling spreading throughout the body. One example of alterations leading to loss of this so-called 'contact inhibition' is the loss of E-cadherin, a key adhesion molecule.

Inducing or Accessing Vasculature. The transport of nutrients poses a challenge for cancer cells as their uncontrolled growth comes with increased energy demand. To enhance delivery of nutrients, cancer cells stimulate the growth of new vasculature. This process called angiogenesis opens new routes for the supply of nutrients and oxygen.

Genome Instability & Mutation. Cancer is greatly dependent on mutations of the genome. Many cancers increase the rate of mutation due to increased sensitivity to mutagenic compounds, disturbance of DNA repair mechanisms, or a combination of both. An example is the loss of function of p53, which is frequently described as 'guardian of the genome'.

Resisting Cell Death. Apoptosis is dependant on extracellular and intracellular signals. Cancer cells that acquire mechanisms to evade these regulatory signals can escape programmed cell death and sustain uncontrolled proliferation.

Deregulating Cellular Metabolism. The unhindered cell growth and proliferation observed in cancers is associated with the need for energy to fuel the increased metabolic activity. To adjust to this demand, cancer cells can change their metabolism. By switching their metabolism to glycolysis, cancer cells can adapt to the anaerobic conditions often found in tumors.

Emerging Hallmarks & Enabling Characteristics. Apart from the aforementioned hallmarks, two additional emerging hallmarks as well as two enabling characteristics have be defined.

Unlocking phenotypic plasticity is considered an emerging cancer hallmark as it can undermine normal progression through predetermined cellular programs. After differentation cells normally enter a life cycle characteristic for the cell type. By dedifferentation to progenitor-like cells, transdifferentation to cells of completely different

morphology, or blocking of differentation cancer cells can escape their fate, avoiding their predetermined cell death.

Senescent cells switch into a mode of lowered metabolism and stop proliferating. Despite their lowered activity, these cells may still play a role in tumor progression, as they have been shown to secrete substances stimulating tumor growth, making them a potential cancer hallmark.

Epigenetic effects may also play a role in tumor progression, as they can lead to acquisition of hallmark capabilities. By reprogramming the genome of a cell, nonmutational epigenetic changes may lead to malignancies and can therefore be considered enabling characteristics.

Another enabling characteristic may be related to cell neighbouring microbiomes. Microorganisms symbiotically associated with tumors comprise a novel field of research with findings suggesting that microorganisms may act as obstacle, but could also play an enabling role in tumor progression.

1.1.3 Global Cancer Burden

Cancer is a leading cause of premature death, *i.e.* of deaths occurring at ages between 30 and 69 years, only being exceeded by cardiovascular diseases.[7] This is due to three major factors. Firstly, advances in medicine, like vaccines and antibiotics, have been contributing to reduced mortality from infectious diseases. Secondly, the demographic shift towards an older society is associated with increased cancer incidence, as accumulation of mutations increases with age. Lastly, cancer incidence is influenced by increased exposure to risk factors such as tobacco smoke, UV light, alcohol, or infectious diseases. These trends can be put into perspective using the human development index (HDI), which allows ranking of countries into four groups, depending on their life expectancy, education, and standards of living. In countries with high to very high HDI, deaths caused by cancer rank first or second among all premature deaths. In medium and low HDI countries cancer frequently ranks third or fourth.

Lung cancer is the most common type of cancer nowadays, which is strongly correlated with tobacco smoking.[8] In women the most common type of cancer is breast cancer.[7] Figure 1 shows the nine most common types of cancer overall in 2022.[9]

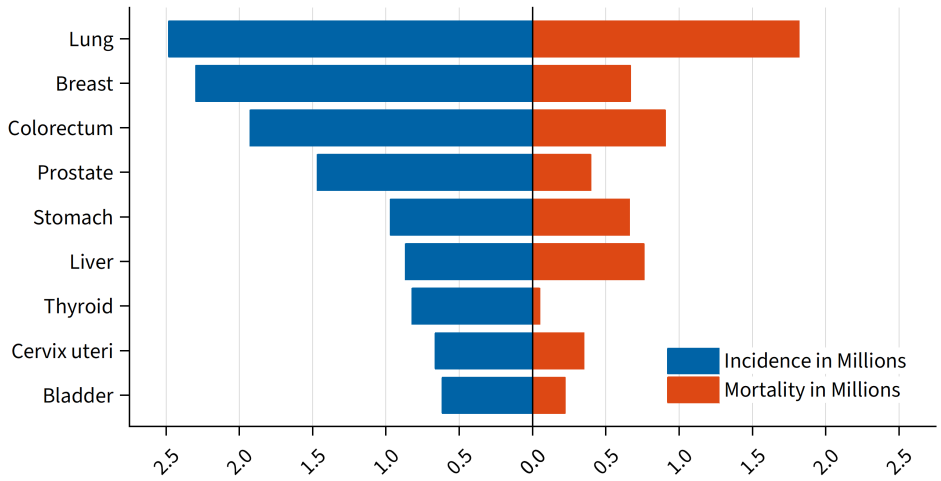

Figure 1: Global cancer incidence and mortality of the nine most common cancers.

1.2 Cancer Treatment

With a yearly death toll in the millions and rising trends, it is no wonder that enormous efforts are being put into cancer research and treatment. Over the millennia cancer treatment has evolved from very basic aids to a multifaceted and interdisciplinary approach, saving thousands of lives each year. Cancer therapy can be classified into several categories, although the actual treatment may utilize more than just one type of therapy.

1.2.1 Therapeutic Approaches

Surgery. Archaeological research indicates that tumors may already have been treated surgically over 4000 years ago,[10] making surgery the oldest cancer therapy we know of today. It is still commonly used to remove tumors or parts thereof, which can serve curative as well as palliative purposes.[11]

Chemotherapy. If cancer develops metastases, surgery may be ineffective or impossible. In such cases chemotherapy can be a sufficient option, as the administered drugs are distributed throughout the body and also effect cancer cells that migrated away from their origin. Chemotherapeutics utilize various mechanism of action against cancer propagation. Prodrugs, for example, are designed to be activated by conditions encountered in the tumor environment. Depending on the choice of the transformative conditions, prodrugs may remain in their inactive state when they are surrounded by normal tissue, preventing unwanted side effects. NAMI-A—shown in Figure 2 **a**—is one example of a prodrug, which entered clinical phase II before being terminated.[12] The

compound 5-fluorouracil (5-FU) is another example of an anticancer agent (Figure 2 **b**), although it utilizes a strategy different to that of NAMI-A. As an antimetabolite 5-FU gets incorporated into DNA instead of nucleobases, leading to faulty DNA and ribonucleic acid (RNA) strands, hindering protein biosynthesis.[13] Temezolomide (Figure 2 **c**), on the other hand, is not incorporated into DNA strands but acts as an alkylating agent. The alkylation of DNA can lead to apoptosis or cell cycle arrest.[13]

Radiotherapy. When cells are exposed to energy-rich radiation they may be destroyed. This principle is used in radiotherapy, which exposes cancer cells to radioactive radiation. Various different methods can be applied. Radiation can enter from the outside, damaging tumors, but also healthy tissue in its path. Radiation may also be used inside the body, wherever a radiation source can be placed in a controlled manner. Furthermore, radioactive atoms can be built into molecules with affinity to certain binding sites, which might be over-expressed in tumors. By accumulating in the tumor these molecules can selectively damage cancer cells and their close environment. Y-Ibritumomab tiuxetan (Figure 2 **d**) is an example of a radiotherapeutic.[14] The monoclonal antibody utilized in this agent attaches itself to the epitope of a cancer cell, while the coordinated ^{90}Y damages cells in close proximity *via* β- decay.

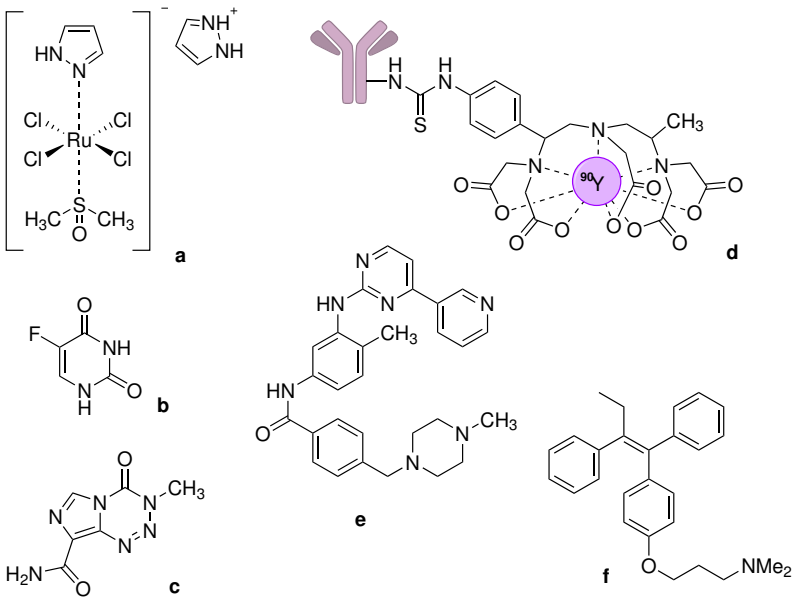

Figure 2: Chemical structures of the anticancer agents NAMI-A (**a**), 5-FU (**b**), temezolomide (**c**), Y-ibritumomab tiuxetan (**d**), imatinib (**e**), and tamoxifen (TAM) (**f**).

Targeted Therapy. Inspired by Ehrlich's more than 100 years old concept of the 'magic bullet',[15] the principles of targeted therapy have experienced a renaissance in recent years. By interference with specific molecular targets that are over-expressed or activated in tumors, cancer growth and its spread can be inhibited. Targets may include surface antigens, receptors, and signalling molecules. Upon interaction with these targets, drugs may block growth-promoting signals, disturb the regulation of the cell cycle, induce apoptosis, or exhibit a combination of these effects.[14] Bevacizumab is an example of anticancer agent utilizing this mode of action. The monoclonal antibody binds to the vascular endothelial growth factor, inhibiting tumor angiogenesis and thereby depriving cancer cells of nutrients. The efficacy of bevacizumab in combination with other agents could be demonstrated for metastatic colorectal cancers.[13] Tyrosine kinase inhibitors comprise another group of well-established targeted therapeutics, with imatinib being one example (Figure 2 **e**). By competing for the ATP binding site of the Abelson tyrosine-protein kinase, it can disrupt signalling pathways present in cancers.[14]

Hormone Therapy. Hormones are signalling molecules, which bind to receptors on their target. By interfering with these regulatory signals, hormone therapy can influence metabolic activity of cancer cells and consequently stop or slow down tumor growth. Tamoxifen (TAM), for example, is a selective estrogen receptor α -positive (ERα^+) modulator used for treating hormone-dependent breast cancer (Figure 2 **f**). The oxidized hydroxyform of the drug binds ERα^+, repressing DNA transcription in cancer cells, resulting in cell death.[16]

Immunotherapy. Evolution has brought forth a number of defense mechanisms, the immune system being one of them. As cancer manages to evade the immune system, its chances of survival increase. Reactivating the immune system poses a promising method to counter unhindered cancer growth. Ipilimumab, for example, is a monoclonal antibody, which decreases some cancers ability to remain unrecognised by the immune system, recruiting T-cells to the tumor-site.[17]

Stem Cell Therapy. Stem cells are embryonic or adult cells with the ability to differentiate into all or various other types of cells and can be used in cancer therapy in several ways. For one, stem cells can regenerate cells compromised by other therapies' side effects. Furthermore, stem cells are drawn to wounded tissue—a condition considered to be chronic in cancers—and thus can be used as carriers to deliver anticancer drugs to the tumor site.[18]

1.2.2 Metal-Based Cancer Therapeutics

Chemotherapeutics constitute a large group of drugs, encompassing a wide variety of compounds. Metal-based anticancer drugs are a diverse group of compounds, utilizing various metals and countless different ligands. Platinum is undoubtedly the most famous example of a metal in anticancer research, although other metals like ruthenium, osmium, and rhenium, to name only a few, increasingly get recognized for their promising tumor-inhibiting effects.

Pt-Based Therapeutics. In 1845 the Italian chemist Michele Peyrone published observations made when treating $PtCl_4$ with ammonia. By deviating from the synthesis procedure of green Magnus Salt, he recognized the formation of a yellow solid. The formed crystals were $[Pt(NH_3)_2Cl_2]$, better known as cisplatin (Figure 3 **a**).[19] When Rosenberg *et al.* showed the inhibitory effects on cell division of *Escherichia coli* exhibited by the Pt compound in 1965, more than a century had passed since its first description.[20] Out of a set of Pt compounds, cisplatin was particularly effective in inhibiting bacterial growth and was subsequently tested for its anticancer activity.[21] The observed growth-inhibiting effect exhibited on cancers in pre-clinical and clinical settings lead to clinical approval of cisplatin, which is still employed to this day. Despite the progress cisplatin represented for cancer therapy, it is by no means a universal remedy for cancer and also faces serious challenges. Cisplatin comes with severe side effects for patients and also struggles with acquired resistance of cancer cells.[22] Side effects may include nephrotoxicity, hematotoxicity, and ototoxicity.[23]

Cisplatin's mode of action is characterized mainly by its interaction with DNA. When reaching the cytosol, the compound is hydrolyzed, with its chlorido ligands acting as leaving groups. The Pt ion consequently forms an adduct with DNA nucleobases, leading to erroneous replication and apoptosis. Another important mode of action is the induction of oxidative stress *via* ROS, leading to apoptosis.

To overcome the severe side effects exerted by cisplatin, various derivatives have been tested over the years, which lead to the development of promising alternatives. Carboplatin (Figure 3 **b**) is such a derivative, which has the advantage of greatly reducing adverse effects. Even though its cytotoxicity is generally lower than that of cisplatin, carboplatin could establish itself globally as clinically used anticancer agent.[24]

Another extensively used Pt-based drug is oxaliplatin (Figure 3 **c**). The eponymous oxalato ligand enhances water solubility compared to chlorido leaving groups. Oxaliplatin achieves similar cytotoxicity while having a favourable safety profile relative to cisplatin.[25] Its mode of action differs from cisplatin by not only inducing DNA damage, but also ribosome biogenesis stress.[26]

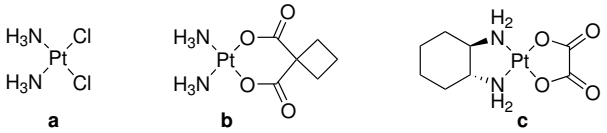

Figure 3: The structures of cisplatin (**a**), carboplatin (**b**), and oxaliplatin (**c**)—three globally approved Pt-based anticancer agents.

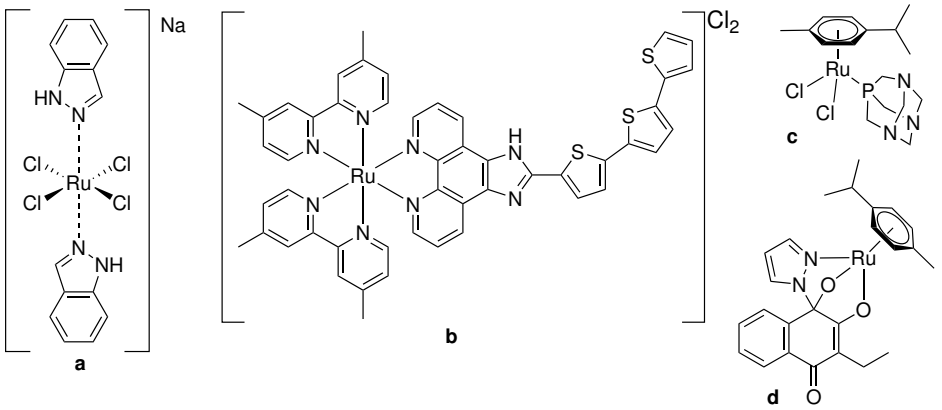

Figure 4: Structures of the Ru-based anticancer agents BOLD-100 (**a**), TLD-1433 (**b**), RAPTA-C (**c**), and a novel, naphthoquinone-based Ru compound with anti proliferative activity in nanomolar range (**d**).

Ru-Based Therapeutics. While representatives of ruthenium compounds are not yet clinically approved, preclinical and clinical studies indicated the potential of Ru complexes. Several compounds entered clinical studies with BOLD-100 being one example (Figure 4, **a**). BOLD-100 is an intravenously administered anticancer agent inducing endoplasmatic reticulum (ER) stress, generation of ROS, and interference with the normal folding of proteins by down-regulation of GRP78. The compound is also believed to interact directly with ribosomal proteins, leading to proliferative inhibition and disturbance of the ER.[27,28]

TLD1433 (Figure 4, **b**) has a somewhat different mode of action. As a photoactivated drug, it is dependent on a light source to be activated (≈ 525 nm). Following activation TLD1433 releases ROS, causing the tumor-inhibiting effect, which has enabled the compounds progression into phase 2 clinical trials.[29]

RAPTA-C (Figure 4, **c**) showed encouraging results in preclinical studies. Investigations revealed anti-metastatic, as well as anti-angiogenic effects while exerting low toxicity *in vitro*.[30]

The RAPTA-family of compounds demonstrated the potential of Ru(II) arene-compounds. One particularly active compound could be synthesized by incorporating a naphthoquinone derivative (Figure 4, **d**), achieving concentrations at which cell growth

is inhibited by 50% (IC_{50}) in the lower nanomolar range.[31] The compound exerted significantly higher cytotoxicity in the SW480 cell line compared to other cell lines tested. The mode of action includes down-regulation of p53 and the consequent inhibition of cell cycle progression in G2/M phase.[32]

Os-Based Therapeutics. Osmium was historically used for its physical properties, namely its hardness and low compressibility, but also for its electrical conductivity, desirable for incandescent lights.[33] Osmium is still investigated for various technical applications such as hard materials,[34] light emitters,[35] or catalysts.[36]

More recently, research expanded to anticancer agents based on osmium. Biochemical interactions of osmium have been known since the beginning of the past century in form of OsO_4 dyes.[37] Osmium inhabits the same group in the periodic table of elements as ruthenium, sharing many of its properties. Many Os analogs of evidently bioactive Ru compounds are synthetically accessible, so it is not surprising that first investigations were focused on analogs of RAPTA-C,[38] NAMI-A,[39] or KP1019.[12,40] Despite similarities to Ru, no Os compound has entered clinical studies yet.

When it comes to coordination chemistry, differences between the two metals can be identified. For one, Os is generally more inert than Ru, meaning it forms more stable, less hydrolysis-prone complexes. This inertness could potentially be utilized to obtain Os model compounds and help illuminate biological interactions of corresponding Ru compounds.[41] Another difference to Ru is the propensity for higher oxidation states. For example, the class of nitridoosmium complexes has Os centers in oxidation state (VI). Substances of this class repeatedly showed cytotoxic effects on cancer cells.[42] Furthermore, Os can influence the coordination-behavior of ligands, as was shown for the Os analog of KP1019. Instead of coordinating *via* 1N, the indazole ligand coordinated Os by the 2N.[12] Cytotoxicity can also be influenced depending on the central metal, as the greater stability of Os complexes is often reason for lowered activity. In other cases, however, changing from Ru to Os can increase activity noticeably, as it was observed with the Os analog of NAMI-A.[39]

Ferrocene. Iron is—like Ru and Os—a group eight transition metal. Nevertheless the ability to coordinate Fe with ligands seen in Ru and Os anticancer agents is limited due to lack of stability. Ferrocene, on the other hand, is a highly stable organometallic compound, which is investigated for potential use in various drugs including anticancer agents.[16]

The first synthesis of ferrocene (Fc) was reported in 1951, when Kealy and Pauson added cyclopentadienyl Grignard reagent to ferrous chloride (Figure 5).[43] Fc is not par-

ticularly cytotoxic. Nevertheless, modification of compounds with ferrocenyl groups has proven to contribute advantageous pharmacological properties. For one, Fc is lipophilic, enhancing the ability of Fc-modified compounds to diffuse through biological membranes and therefore reaching potential targets inaccessible for more polar compounds. Furthermore, Fc derivatives may induce the formation of ROS. Research conducted with MCF7 cells showed that ferrocenium salts with sufficient aqueous stability inhibit cell growth *via* ROS-induced DNA damage. The proposed mechanism of action is initiated by degradation in aqueous solvent (1). A Haber–Weiss-type reaction (2, 3) and subsequent Fenton reaction (4) lead to the generation of hydroxyl radicals.[44]

$$2[Fe^{III}(Cp)_2]^+ + nH_2O \longrightarrow [Fe^{II}(H_2O)_n]^{2+} + [Fe^{II}(Cp)_2] + 2Cp^\bullet \quad (1)$$

$$[Fe^{II}(H_2O)_n]^{2+} + O_2 \longrightarrow [Fe^{III}(H_2O)_n]^{3+} + O_2^{\bullet-} \quad (2)$$

$$2O_2^{\bullet-} + 2H_2O \longrightarrow O_2 + H_2O_2 + 2OH^- \quad (3)$$

$$[Fe^{II}(H_2O)_n]^{2+} + H_2O_2 \longrightarrow [Fe^{III}(H_2O)_n]^{3+} + OH^- + OH^\bullet \quad (4)$$

Fc has also proven to increase the efficacy of existing therapeutics. The anti-malarial agent chloroquine (CQ), as shown in Figure 6 **a**, blocks the digestive vacuole of pathogenic parasites such as *Plasmodium falciparum,* leading to their death. The efficacy of this agent, however, is compromised by the emergence of CQ-resistance. A multi modal approach can help relief this circumstance, as the ferrocene derivative ferroquine (FQ) demonstrates (Figure 6 **b**). Apart from a similar mode of action observed in CQ, FQ also exhibits anti-malarial properties by means of oxidative stress.[45]

Fc derivatives have also been investigated for use in cancer therapy. One particularly interesting group of compounds are Fc derivatives of TAM, called ferrocifens (Figure 6 **c**, **d**). As important as it may be for the therapy of hormone-dependent breast cancer, TAM is inactive in hormone-independant breast cancer, which is responsible for about one third of breast cancer incidences. Ferrocifens may deliver means to tackle both hormone-dependant and -independant breast cancers by introducing induction of ROS as an additional mode of action.[46]

Apart from its ROS-generating function, ferrocenyl groups may also be used as bioisosteres, modulating the affinity of compounds towards binding pockets of re-

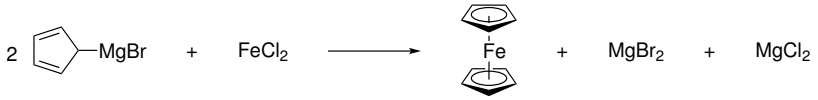

Figure 5: Synthesis of Fc as first conducted by Kealy and Pauson in 1951.

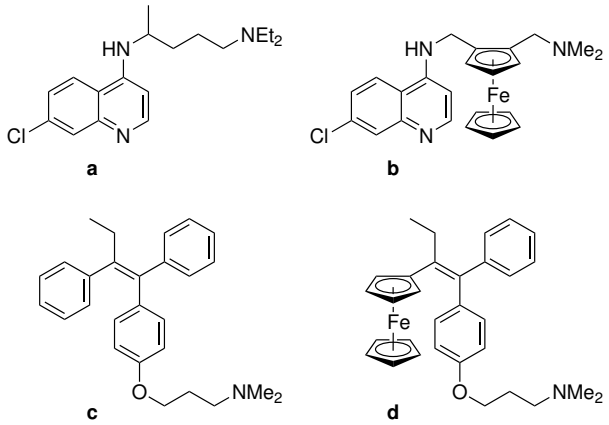

Figure 6: Chemical structures of the anti-malarial agents chloroquine (**a**) and ferroquine (**b**), as well as of the anticancer agents tamoxifen (**c**) and ferrocifen (**d**).

ceptors. For example, the addition of ferrocenyl groups may increase affinity towards receptor binding sites, as was demonstrated for certain G-protein-coupled receptors.[47]

Another way of utilizing Fc is in the form of an antenna for photoactivated therapeutics, as was shown for various ferrocenyl-modified compounds. Some Fc-containing complexes exhibit higher cytotoxicity in cancer cells than their Fc-free analogs when activated with visible light.[16] The mechanistic role of Fc has yet to be fully elucidated, but first insights suggest that it may act as a photo-initiator, leading to ROS-generation *via* a Fenton-like mechanism.[48]

1.2.3 Reactive Oxygen Species

As the previous sections have demonstrated, ROS are an important aspect in drug design. The following section elucidates what ROS are, why oxygen plays such an important part in radical mechanisms and how it does so.

With a ratio of about 21%, O_2 is the second most abundant element of the terrestrial atmosphere. The predominant form of atmospheric O_2 is triplet oxygen, which is characterized by two unpaired electrons of parallel spin, residing in the anti-bonding π^* orbitals. These partially filled orbitals offer space for additional electrons, as illustrated in Figure 7, enabling the reduction of triplet oxygen to less stable, more reactive forms: so called reactive oxygen species.

Depending on their concentration and localization, ROS are involved in important physiological processes, but also contribute in reactions damaging cellular structures. Low concentrations of ROS may stimulate cell proliferation and gene expression, while higher concentrations induce damage to lipids, proteins, and nucleic acids. In the human body, ROS are typically generated either by sources of high energy, e.g. UV radi-

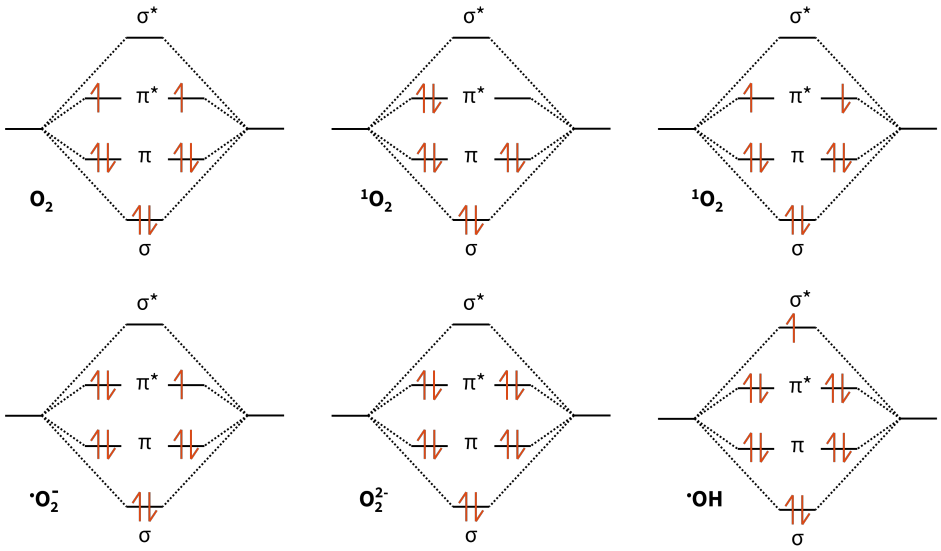

Figure 7: The molecular orbital diagrams of common ROS are shown. While the relatively stable triplet oxygen (**O_2**) has the same bond order as the two types of singlet oxygen (**$^1O_2$**), the opposite electron spins in the latters' π^* orbitals are energetically disfavoured, decreasing the species' stability. Superoxide (**$\cdot O_2^-$**), peroxide (**O_2^{2-}**), and the hydroxyl radical (**$\cdot OH$**) decrease in stability in this order due to an increasing electron number in anti-bonding orbitals and therefore decreasing bond order.

ation, or metabolic pathways. The initially generated superoxide ($\cdot O_2^-$) can be considered the primary ROS, as it can further react, giving rise to secondary species. It may be oxidized to O_2 either spontaneously or enzymatically, or reduced to its peroxide form (O_2^{2-}). The highly reactive hydroxyl radical can then be formed from H_2O_2 in the metal-catalysed Fenton reaction, as shown in reaction scheme (4).[49]

When the Fenton reaction was first discovered, it was described as a reaction of H_2O_2 with Fe(II), giving rise to the hydroxyl radical.[50] Today we know that other metals such as titanium and copper are also able to propagate Fenton-like reactions, although iron remains the predominant mediator of such reactions in the human body. The produced hydroxyl radical is extremely reactive and will interact rapidly with most biological molecules, thus the secure storage of iron is of vital importance to an organism. This task is fulfilled by proteins such as ferritin or Fe-S cluster proteins.[51] Ferritin, as the major storage protein for iron, can release Fe(II) following reduction of its ferric core. This release can be mediated *via* different means including enzyme activity, or energy rich radiation.[52]

1.3 Phases in Cancer Research

Compounds need to undergo thorough regulated testing in order to be introduced to the market, advancing through various stages of evaluation before they can be approved for use in humans. The following paragraphs will summarize the initial preclinical phase, as well as the four phases of clinical trials on a anticancer agent's way to clinical approval.

1.3.1 Preclinical Research

Countless potential anticancer drugs get synthesized or isolated every year. Single research groups can produce whole catalogues of substances, consisting of hundreds or even thousands of compounds, not to mention the enormous output generated by companies. To evaluate the most promising out of the many drug candidates, a preclinical phase of high throughput is desirable. This stage aims at gaining first insights into a substance's behavior in biological systems, such as cancer cell cultures or animal test models.

Cell Culture. Since the establishment of the HeLa cell line in the 1950s,[53] cell culture emerged as indispensable tool for preclinical research. By supplying isolated cells with needed nutrients, maintenance and growth outside of the donors can be achieved. Some cells—predominantly cancer cells—can evade normal cell cycle behavior and gain replicative immortality, making them proper candidates for the establishment of cell lines. Many kinds of tissues and cancers are represented by multiple available cell lines, enabling targeted research and globally comparable results. Ease of cultivation and relatively low cost, as well as abundance of available assays and fewer ethical concerns compared to animal testing, make cell culture techniques a predominant tool in preclinical research.

Animal Models. Despite ethical issues and higher cost, the use of animal test models sometimes is without alternatives. Utilities of animal models in cancer research include the investigation of pathophysiology, identification of novel therapeutic compounds, exploring efficacy of combined therapies, and studying mechanisms of drug resistance.[54]

1.3.2 Clinical Research

A substance of promising anticancer activity may enter clinical trials, opening the opportunity for approval by the respective authorities. The lengthy process leads through various phases listed below.[55]

Phase 0. The initial stage of clinical trials aims at gaining first insight into how a treatment acts on patients. This stage generally needs fewer participants and only low doses of a compound are administered.

Phase 1. The following phase's purpose is to determine a recommended dosage of the tested compound. Safety and maximal tolerated concentration of a compound is pursued *via* dose escalation studies in a relatively small group of patients.

Phase 2. The recommended dosage determined in phase 1 is then tested for its efficacy. The general goal is to achieve greater anticancer activity than possible with existing treatments for a specific type of cancer.

Phase 3. If a substance progresses successfully through the previous phases, the therapy is tested in a larger number of participants, ranging from hundreds to thousands. In these comparative studies, compounds are tested alongside other treatments, including the best standard treatment. If a drug candidate offers superior efficacy over the standard treatment, it may be approved by the respective authorities.

Phase 4. Following approval, therapeutics are administered to an even greater number of patients and are monitored over a prolonged period of time to gain further knowledge about the effects of a drug.

1.4 Cell Culture Techniques

A great variety of compound properties can be determined in cell culture. The following paragraphs summarize a few essential techniques and assays frequently used in preclinical studies.

1.4.1 Subcultivation

Adherently growing cells—typically cultivated on the bottom of suitable flasks or dishes—are limited in their growth by the available area of their containing vessel. In cell culture, when cells get confluent, *i.e.* the available area is fully covered, cells will no

longer proliferate exponentially. As it is desirable to harvest only cells undergoing exponential growth (log phase) for the usual experimental setup, cells need to be thinned out before reaching confluency. This thinning out of cells is referred to as subculturing or passaging of cells.

1.4.2 MTT Assay

When cells are exposed to cytotoxic substances, their proliferative behavior may be disturbed. The growth inhibition exerted by a compound—expressed as IC_{50} values—can give first insight into its potential as an anticancer agent. Since first published in 1983,[56] the 3-(4,5-dimethylthiazol-2-yl)-2,5-diphenyl-2H-tetrazolium bromide (MTT) assay has established itself as one of the standard methods for assessing cell viability. It allows the estimation of metabolic activity by colorimetrically measuring the intracellular conversion of MTT to formazan crystals. By applying different concentrations of a compound and fitting the respective optical densities (ODs) in percent of the untreated control to a concentration-effect curve, the IC_{50} can be interpolated.

1.4.3 DCFH-DA Assay

The induction of ROS is a common facet in the mode of action exerted by therapeutic agents.[16,57] A routine method used to quantify ROS generation exerted by a compound, is the 2',7'-dichlorodihydrofluorescein diacetate (DCFH-DA) assay. This assay utilizes the non-fluorescent precursor DCFH-DA, which readily penetrates cell membranes. Once inside a cell, acetate groups are cleaved by esterases to give DCFH. In the presence of certain ROS, DCFH is oxidized to its fluorescent form 2',7'-dichlorofluorescein (DCF).[58,59] The amount of DCF can be measured fluorimetrically at a wavelength of 516 nm, allowing the estimation of ROS responsible for oxidation.

1.4.4 Cellular Accumulation

A compound's cytotoxicity does not give any indication on bioavailability. To set IC_{50} values into perspective, it is useful to determine a substance's cellular accumulation. For metal complexes, the cellular uptake correlates with the presence of the coordinated metal in the treated cells. The amount of a given metal can be quantified using inductively coupled plasma (ICP)-mass spectrometry (MS), as was first demonstrated in 1983.[60]

2 Results and Discussion

2.1 Aim of this Thesis

Os and Ru are promising metals for use in potential anticancer agents for reasons outlined in 1.2.2. As was previously shown, bioactive Ru complexes can be synthesized under microwave conditions.[31] The aim of this thesis is the synthesis of four Os complexes under similar conditions, as well as their characterization. The assessment of the synthesized complexes' biological activity, as well as of their Ru analogs and free ligands—shown in Figure 8—in various biological assays was a further objective.

2.2 Complex Synthesis

The syntheses of **1**–**4** were conducted as one-pot reactions under microwave conditions, according to the reaction scheme in Figure 9. The respective quinones and Os-dimer (Figure 10) were dissolved in methanol (MeOH), followed by the addition of triethylamine (NEt_3). By utilizing the Biotage® Initiator+ microwave system and reaction times of 20 min, yields between 37% and 79% could be achieved. Flash chromatography was possible only when adding NEt_3 or ammonia (NH_3) solution to the mobile phase to account for the products sensitivity towards acidic conditions.

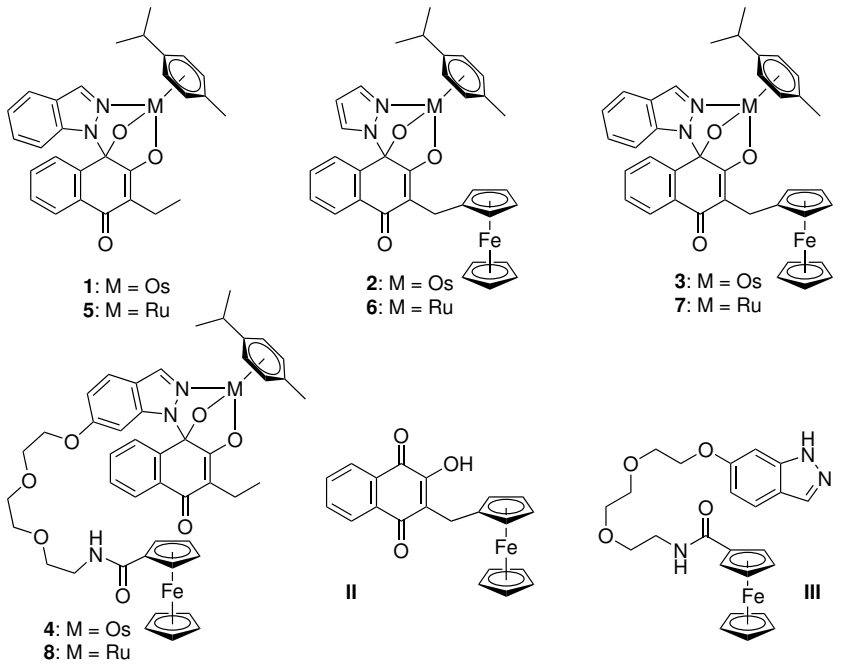

Figure 8: Ru and Os complexes, as well as free ligands considered in this thesis.

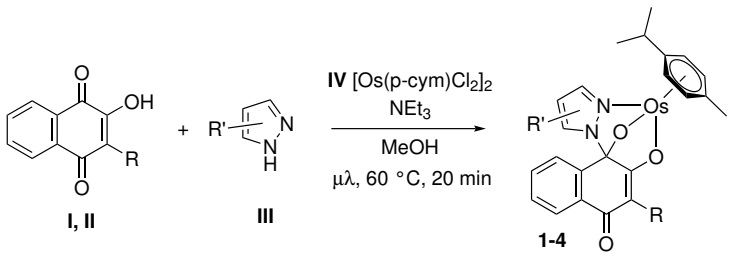

Figure 9: Procedure used for the syntheses of compounds **1**–**4**.

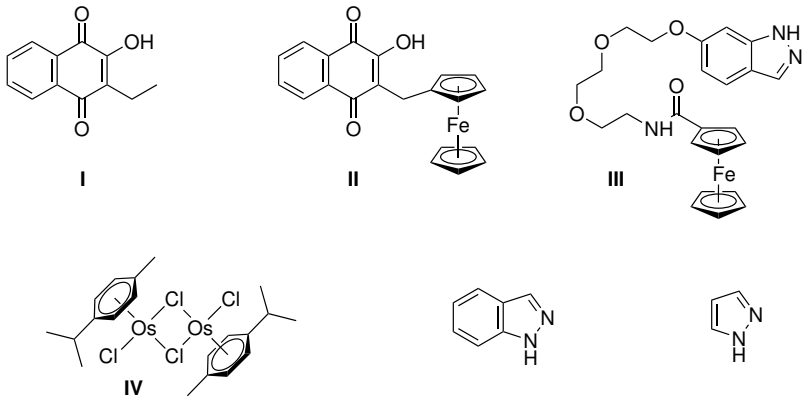

Figure 10: Reagents used for the conducted complex syntheses.

The utilized one-pot reaction is not only easily accessible, it also enables much shorter reaction times, when compared to conventional synthesis routes.[61,62] Yields indicate potential for optimization, as the Ru counterparts of the synthesized Os complexes generally showed better yields, which may be testament to the greater inertness of the Os analogs.

2.3 Characterization

NMR Spectroscopy. For each complex, a set of nuclear magnetic resonance (NMR) spectra was recorded in deuterated dimethyl sulfoxide (DMSO). By interpreting ^{1}H, ^{13}C, correlation spectroscopy (COSY), heteronuclear single quantum coherence (HSQC), and heteronuclear multiple bond coherence (HMBC) spectra, all signals could be assigned to their respective nuclei, as demonstrated for **4** (Figure 11), confirming the formation of the desired products. Peak labels for the arene ligand are **a**–**g**, the semiquinone-part of the tridentate corresponds to labels **1**–**12**, **i**–**vii** are the labels of the indazole group, and the Fc-containing polyethylene glycol (PEG) linker is labelled **a'**–**l'**.

All complexes have in common various aromatic motifs, which resulted in overlapping signals. The formation of **1**–**4** was confirmed by the missing OH-signal of coordinat-

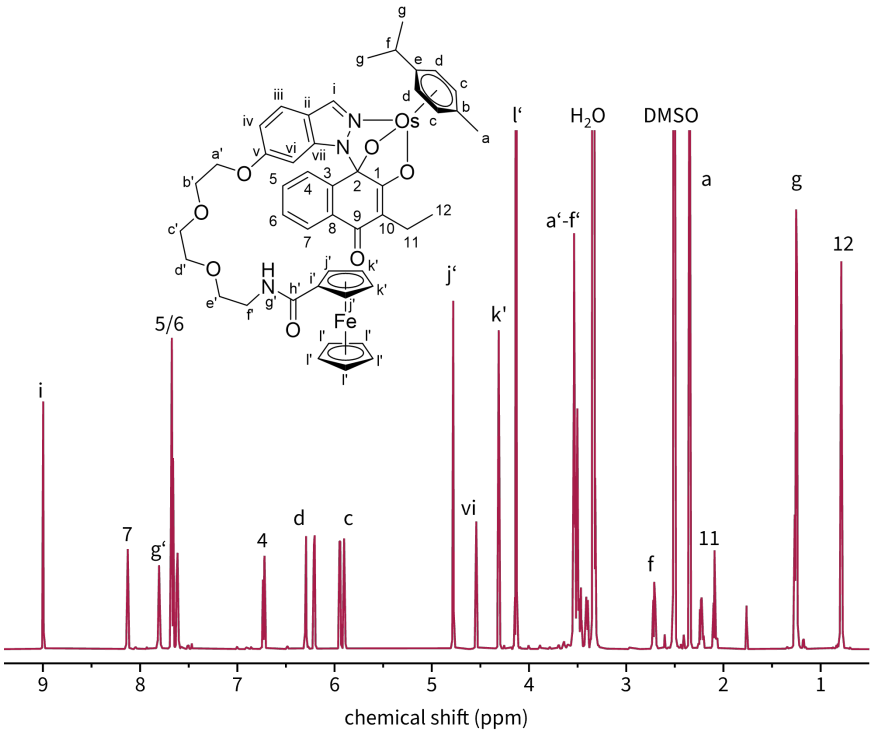

Figure 11: ^{1}H–NMR spectrum of **4**.

ing naphthoquinone OH-group, as well as by the four signals observed for the p-cymene ligand, which are only observed when coordinated to the central atom. Between 9.00 and 6.50 ppm lie ^{1}H–NMR signals corresponding to the aromatic parts of the tridentate ligand like **4**–**7**, **i**, and other protons originating from the added diazole. Only **vi** is an outlier with shifts below 5.5 ppm. The corresponding carbon signals (Figure 12) are tightly packed between 120 and 140 ppm. Special to **4** is only the additional amine proton **g'**, which lies at about 7.8 ppm. The two carbonyl signals at 180 ppm in the ^{13}C–NMR spectrum are overlapping perfectly, making them prone for misinterpretation. Characteristic for this type of N,O,O chelated complexes is the carbon signal around 100 ppm, corresponding to the hemiaminal **2**.

Signals induced by the aromatic protons of p-cymene were found in the region around 6.00 ppm. Between 3.60 and 4.80 ppm lie ferrocene signals, among them an intense singlet accounting for the five equivalent protons of the unmodified cyclopentadienyl ring. The corresponding peak at around 69.3 ppm in the ^{13}C–NMR spectrum is also of high intensity. The remaining ferrocene signals are grouped with p-cymene and PEG signals between 65 and 70 ppm.

For **4**, a signal-rich region can be observed in close proximity to the water peak at 3.3 ppm, which is due to 12 protons situated on the PEG linker. Shifted high field with regards to the water peak lie only the non-aromatic protons such as **a**, **g**, and **11**.

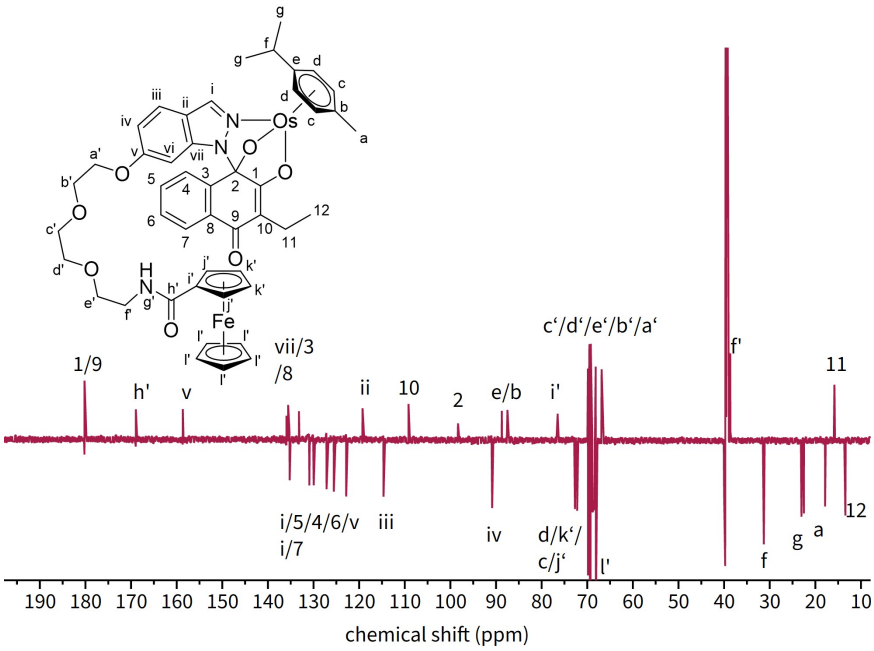

Figure 12: ^{13}C–NMR spectrum of **4**.

Mass Spectrometry. Compounds **1**–**4** were characterized using MS, giving the expected molecular weights and showed the respective isotopic pattern of the Os centre. The mass spectrum in Figure 13 shows patterns characteristic of Os-containing compounds. Peaks at doubled m/z indicate the formation of dimers, while peaks with additional +23 m/z corresponded to ^{23}Na adducts.

Elemental Analysis. Compounds **1**–**4** were investigated for their elemental composition. Compounds **1** and **4** exhibit hygroscopic properties, as can be seen from the elevated oxygen content in tables 5–8, which may be due to water in the samples. When corrected for their water content, all compounds were within maximum deviation of 0.4% from the theoretical composition for C, H, N, and O.

Stability Measurements. Compounds **1**–**4** were dissolved in DMSO and the so-obtained stock solutions were added to quartz cuvettes containing Dulbecco's Phosphate Buffered Saline (PBS) (pH 7.4) and 4 µL per mL DMSO. UV–vis absorption spectra were recorded every 30 min over a period of 48 h. Unfortunately, **3** precipitated over time. In Figure 14 the UV–vis absorption spectrum of **1** can be seen, which shows slight decrease of absorption over time especially visible at the local maximum at 370 nm. A peculiar local minimum can be observed for initial measurements around 280 nm, which gets less pronounced for the second half of the measurements duration. Isos-

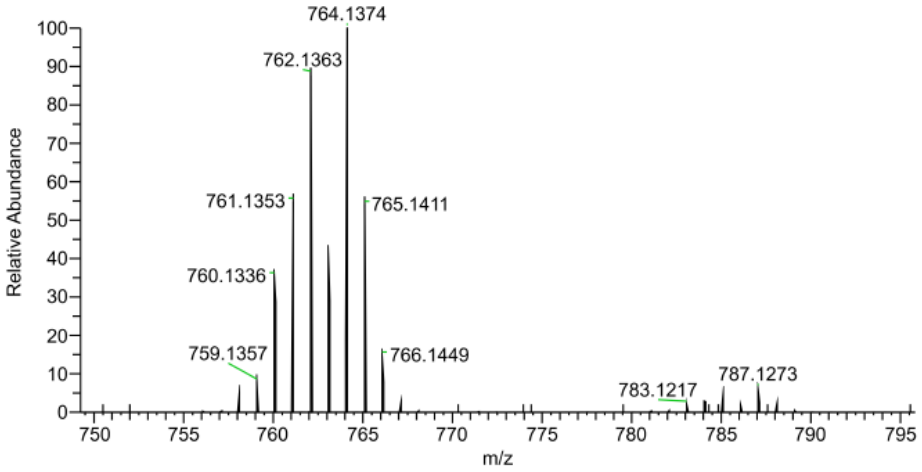

Figure 13: Mass spectrum of **2**.

bestic points exist at wavelengths of 260, 295, and 425 nm, indicating conversion of species over time. Comparable observations can be made with the absorption spectrum of **2** (Figure 15). A pronounced isosbestic point at 340 nm and the shift of absorption to shorter wavelengths may indicate the conversion into other species. Another isosbestic point is located at 425 nm. The absorption spectrum of **4**, as can be seen in Figure 16, shows a local minimum at 290 nm, comparable to the minimum observed for **1**. Isosbestic points can be observed at 260 and 305 nm, while none exists at 425 nm. The absorption only sees minor changes over 48 h, indicating sufficient stability under the measurement conditions. Figure 17 shows the decrease of absorption over 48 h for **1**, **2**, and **4**, normalized to each compounds highest absorption at a wavelength of 370 nm. While the absorption of **4** remains above 95% throughout the whole measurement, the absorption of **1** and **2** drop to about 90% after 48 h. The decrease in absorption may be due to conversion into other species or precipitation. One possibility to determine the generation and identity of conversion products in the future could be the use of liquid chromatography (LC)-MS.

Crystal Structures. For compounds **2** and **3** single crystals could be grown *via* slow diffusion from dichlormethane (DCM) and n-hexane (nHex). The crystal structures were determined using single crystal X-ray diffraction (SXRD) and can be seen in Figure 18. Compound **2** crystallized in the triclinic space group P-1 while for **3** the monoclinic space group $P2_1/c$ was observed. Selected bond lengths are listed in table 1 with O2 being the hemiaminal oxygen.

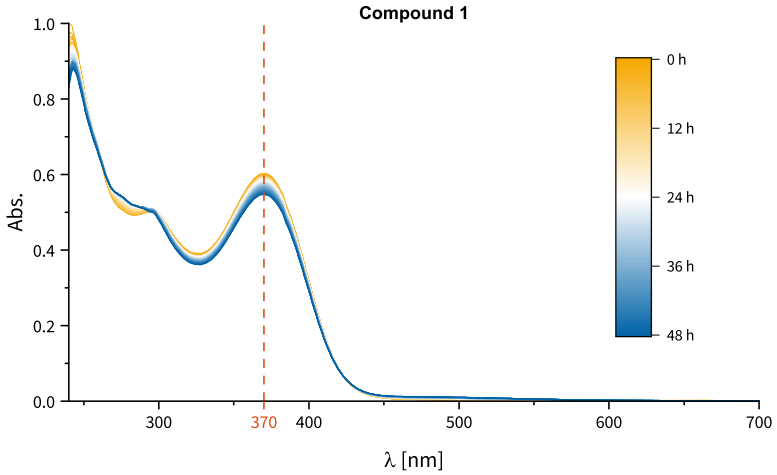

Figure 14: UV–Vis absorption spectrum of **1** in PBS (pH 7.4), recorded in 30 min intervals for 48 h.

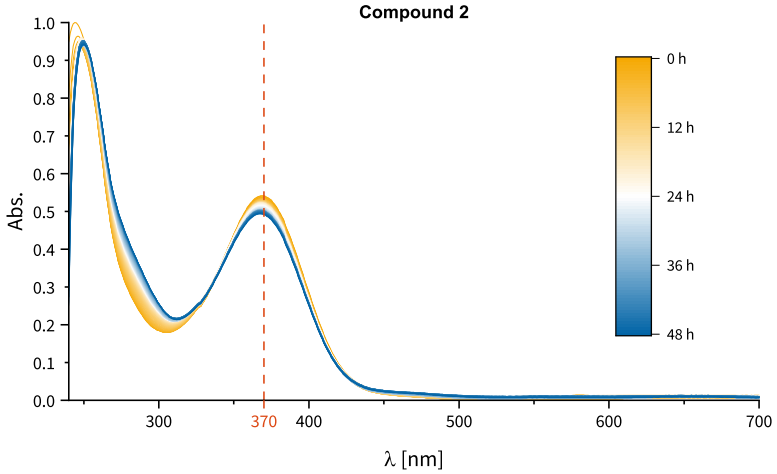

Figure 15: UV–Vis absorption spectrum of **2** in PBS (pH 7.4), recorded in 30 min intervals for 48 h.

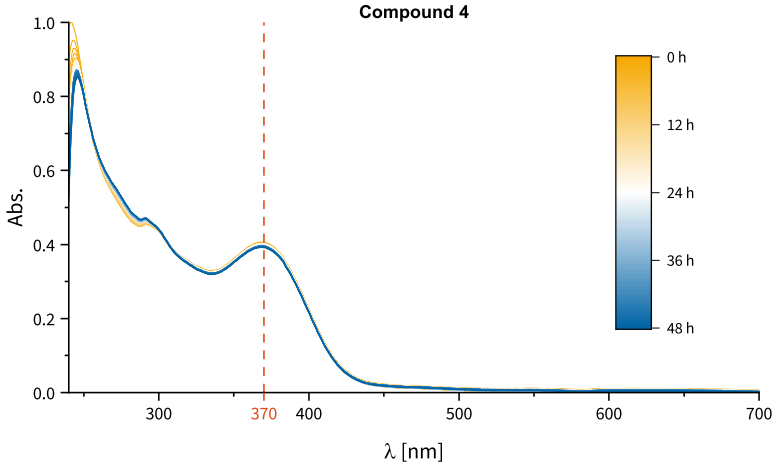

Figure 16: UV–Vis absorption spectrum of **4** in PBS (pH 7.4), recorded in 30 min intervals for 48 h.

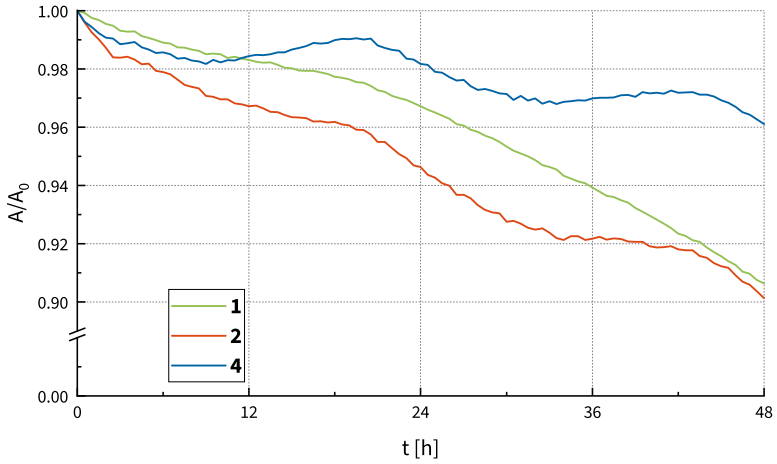

Figure 17: Decrease of absorption of **1**, **2**, and **4** over 48 h. The curves are normalized to the highest absorption at 370 nm wavelength.

Table 1: Selected Distances to Central Atom in Å

compound	Os—O1	Os—O2	Os—N	Os—p-cym
2	2.129	2.061	2.108	1.668
3	2.099	2.066	2.141	1.659

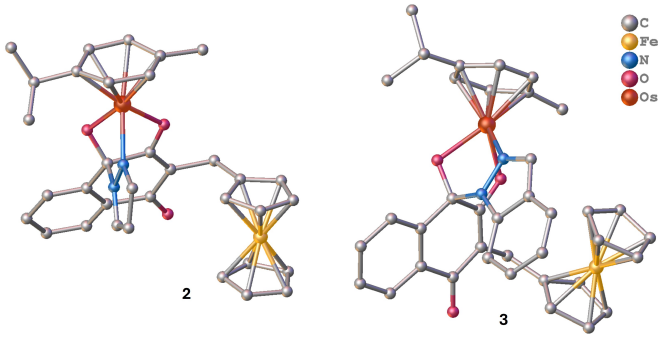

Figure 18: Crystal structures of **2** and **3**. Hydrogen atoms were omitted for clarity.

2.4 Biological Studies

Preclinical studies are required for any anticancer drug before entering clinical investigations. Such studies may utilize various organisms and cells to give first insight into potential drugs' behavior in biological systems. A great number of assays is available to enable multifaceted determination of countless properties, such as cytotoxicity, cellular accumulation, induction of ROS, and DNA damage, to mention only a few. In this work emphasis was put on three *in vitro* assays, namely the MTT assay, the DCFH-DA assay, and the cellular uptake. This combination of assays allows the validation of whether or not the addition of Fc groups has an effect on ROS levels and how this may relate to cytotoxicity and the amount of a compound present in cells.

2.4.1 MTT Assay

Compounds **1**–**8**, **II**, and **III** were applied to CH1/PA-1, SW480, A549, and CT26 cells for 96 h. After incubating cells with MTT solution for 4 h, concentration-effect curves were obtained by plotting ODs against compound concentrations. The IC_{50} was determined for each substance-cell line combination *via* point-to-point interpolation and averaged over 3–5 experiments. An exemplary curve can be seen in Figure 19 while all remaining curves can be found in the appendix. The interpolated IC_{50} values are documented in Table 2.

The ligand **II** shows some cell growth inhibitions with IC_{50} values in the micromolar range, which is markedly lower than observed for the Fc-free naphthoquinone derivative.[31] For ligand **III** no IC_{50} values could be determined with a maximum applied concentration of 100 µM.

Compounds **5** and **8** show IC_{50} values in the nanomolar range in SW480 cells, comparable to complexes tested previously.[31] The effects of **6** and **7** on SW480 cells are of

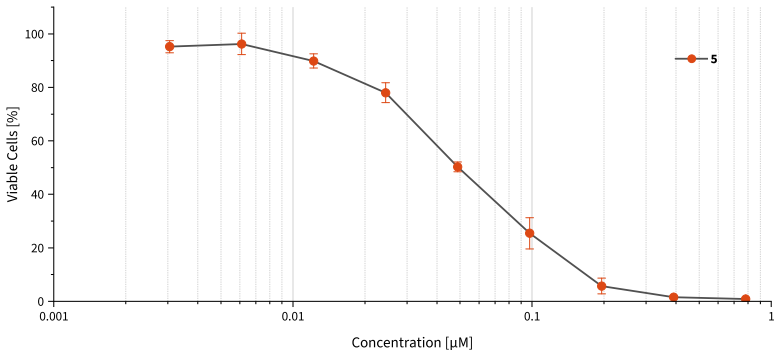

Figure 19: Concentration–effect curve of **5** in SW480 cells.

Table 2: Interpolated IC_{50} Values (Means ±Standard Deviation)

Compound	CH1/PA-1 [µM]	SW480 [µM]	A549 [µM]	CT26 [µM]
1	17.02 ± 3.27	0.30 ± 0.02	2.36 ± 0.22	27.81 ± 2.90
2	1.63 ± 0.23	1.52 ± 0.30	3.55 ± 0.60	0.55 ± 0.07
3	0.27 ± 0.03	0.68 ± 0.10	0.79 ± 0.16	0.14 ± 0.01
4	6.93 ± 1.50	0.25 ± 0.07	2.25 ± 0.40	7.63 ± 0.56
5	16.24 ± 4.29	0.050 ± 0.002	0.76 ± 0.12	1.51 ± 0.40
6	2.98 ± 0.69	0.51 ± 0.05	2.19 ± 0.11	1.27 ± 0.18
7	0.59 ± 0.15	0.26 ± 0.02	1.07 ± 0.09	0.33 ± 0.05
8	4.58 ± 1.84	0.059 ± 0.017	1.29 ± 0.30	3.83 ± 0.29
II	15.27 ± 1.45	32.96 ± 3.70	38.15 ± 1.77	7.80 ± 1.58
III	≈100 ± /	/ ± /	/ ± /	/ ± /

lower intensity, suggesting that the semiquinone's ethyl group is responsible for the increased activity. The greater cytotoxicity in SW480 cells can also be observed with the Os analogs **1** and **4**, although less pronounced.

Although the highest activities were observed in the SW480 cell line, not all compounds were most active in this cell line. For example, **3** and its corresponding free ligand **II** exerted higher cytotoxicity in CH1/PA-1 and CT26 cells. Remarkably, IC_{50} values of **2** and **3** in CT26 cells, which were 1–2 orders of magnitude lower than those of **1** and **4**. Furthermore, these two substances were more active in both CH1/PA-1 and CT26 cells than their Ru counterparts, indicating the enhancement of selectivity towards those cell lines due to the presence of Fc, the change of the central atom to Os, or a combination of both.

2.4.2 DCFH-DA Assay

Compounds **1**–**8**, **II**, and **III** were applied to SW480 cells pretreated with DCFH-DA solution. The formation of the fluorescent DCF species was fluorimetrically measured over 2 h. By comparing to a negative control, the redox behavior of the tested compounds was derived. The measured intensities relative to the negative control are shown in Table 3 for the highest concentrations applied.

None of the metal complexes showed elevated ROS levels, with the exception of a slight increase for **6**, which a Welch's t-test ($p > 0.05$) revealed to be insignificant. The only significant increase was observed for **II**, which showed nearly threefold increase in fluorescent intensity, indicating oxidative potential.

Table 3: Relative Fluorescent Intensities

Compound	T/C		
1	0.68	±	0.41
2	0.55	±	0.21
3	0.53	±	0.26
4	0.59	±	0.30
5	0.58	±	0.20
6	1.13	±	0.72
7	0.68	±	0.22
8	0.80	±	0.40
II	2.96	±	0.85
III	0.72	±	0.13

2.4.3 Cellular Accumulation

As the utilized procedure did not allow for the measurement of Os content due to the generation of volatile OsO_4, only compounds **5**–**8** were applied to SW480 cells (5 µM) for 2 h. The treated cells were washed and then lysed with HNO_3, and ruthenium content was quantified using ICP-MS. The blank-corrected amounts of Ru are shown in Table 4. Cells treated with **5** and **8** showed pronounced uptake of Ru of 239.9 ± 50.4 and 219.2 ± 15.2 fg per cell, respectively. These two compounds also showed the highest cytotoxicity in MTT assays in the SW480 cell line. Compounds **6** and **7** showed much lower accumulation. These results indicate that the ethyl group of the semiquinone may be crucial for this compound class to exert its cytotoxic effects on SW480 cells. As was shown previously,[31] compounds bearing this ethyl group are of much greater cytotoxicity than even slightly modified derivatives. The addition of Fc influenced the uptake of compounds only when situated at the naphthoquinone-position, while PEG-linker and Fc attached thereon did not significantly influence the accumulation in SW480 cells.

Table 4: Ruthenium Content in Treated Cells

Compound	Ru [fg/cell]		
5	239.9	±	50.4
6	29.4	±	10.9
7	66.1	±	8.1
8	219.2	±	15.2

3 Experimental Section

The experiments conducted for this thesis can be divided into two groups. The first group of experiments regards the synthesis of four Os complexes. The materials and methods used, as well as general and detailed procedures are presented alongside the characterization of the obtained products.

The second group of experiments deals with the assessment of biological data. The behavior of the synthesized Os complexes in various cancer cell lines was examined using three assays. These assays give insight into growth inhibition, generation of ROS, and cellular uptake.

3.1 Statistical Methods

To determine if two means differ significantly, Welch's t-tests were performed ($\alpha = 0.05$).

3.2 Complex Syntheses and Characterization

3.2.1 General Remarks

All solvents were commercially available and were used as delivered. Reagents were available from commercial suppliers, except for **I**–**IV**, which were synthesized at the Faculty of Chemistry, University of Vienna. Reactions were conducted using a Biotage® Initiator+ microwave system. Products were purified *via* medium pressure liquid chromatography (MPLC) utilizing the Biotage® Isolera™ system (silica gel, 40–63 µm).

All analytical procedures were conducted at the Faculty of Chemistry, University of Vienna. For the recording of NMR spectra, a Bruker Avance III 600 (^{1}H: 600.18 MHz, ^{13}C: 150.93 MHz) or Bruker Avance III HD 700 (^{1}H: 700.40 MHz, ^{13}C: 176.12 MHz) spectrometer were used, with the samples dissolved in deuterated DMSO. Mass spectra were generated by the faculty's mass center using a Bruker maXis ESI-QqTOF in positive ionization mode. The elemental compositions were determined by the microanalytical laboratory using an Eurovector EA 3000 CHNS-O analyser. Solubility was determined by diluting stock solutions (m ≈ 1 mg) in 10 µL steps, until addition of 10 µL of stock solution to 990 µL PBS buffer would no longer lead to precipitation. If possible, single crystals were obtained by liquid-liquid diffusion in DCM/nHex and crystal structures were determined using SXRD.

3.2.2 General Procedure

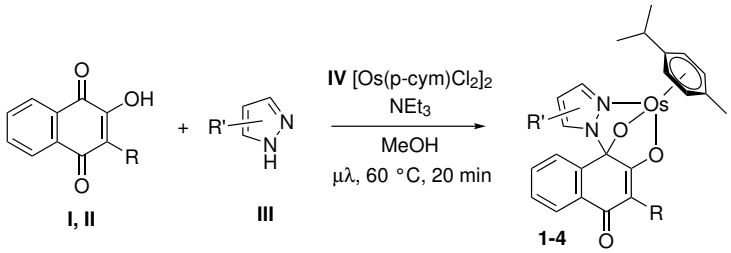

Figure 20: General procedure for the synthesis of the investigated Os complexes.

Osmium dimer (0.15 mmol, 1.0 equivalent (eq)) was weighed into a microwave suitable vial and was dissolved in 20 mL of MeOH. After addition of **I** or **II** (0.29 mmol, 1.9 eq); indazole, pyrazole, or **III** (0.29 mmol, 1.9 eq) was added to the mixture. Following 5 min of stirring at room temperature (r.t.), NEt_3 (0.90 mmol, 6.0 eq) was added to the yellow-green suspension, turning the colour to dark-red. The vial was capped and the mixture was heated to 60 °C for 20 min under microwave conditions. The mixture was cooled to r.t. and solvent was removed under reduced pressure. The pure product was obtained *via* flash chromatography and dried overnight at 50 °C under high vacuum.

3.2.3 3-Ethy-4-oxo-(1H-*κN*2-indazole-1-yl)-(1,4-dihydronaphtalene-1,2-bis-(olato)-*κO*1-*κO*2)(*η*^{6}-p-cymene)osmium(II) (1)

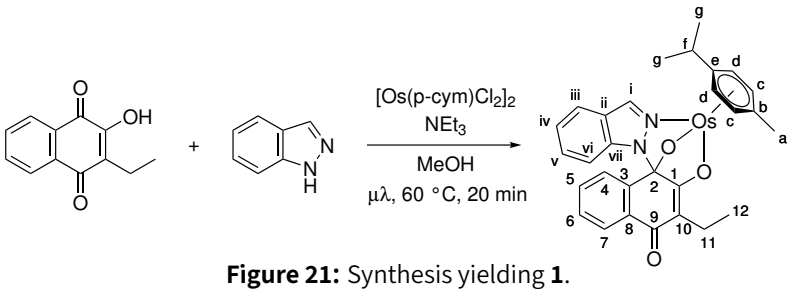

Figure 21: Synthesis yielding **1**.

The synthesis was conducted according to the general procedure, using **IV** (121 mg, 0.153 mmol, 1.00 eq), **I** (35 mg, 0.30 mmol, 2.0 eq), indazole (60 mg, 0.29 mmol, 1.9 eq), and NEt_3 (127 µL, 92 mg, 0.91 mmol, 6.0 eq). The pure product was obtained *via* flash chromatography (applied in DCM, 25 g silica, 80% ethyl acetate (EtOAc)/nHex, 5% NEt_3), as a beige powder (125 mg, 64%).

^{1}H–NMR (600.18 MHz, DMSO-d6) δ 9.16 (d, J = 0.9 Hz, 1H, $C_{arom.}$, **i**), 8.11 (dd, J = 7.9, 1.4 Hz, 1H, $C_{arom.}$, **7**), 7.84–7.79 (m, 1H, $C_{arom.}$, **iii**), 7.68 (dd, J = 7.5, 6.1 Hz, 1H, $C_{arom.}$, **5**), 7.67–7.65 (m, 1H, $C_{arom.}$, **4**), 7.59 (ddd, J = 7.4, 7.4, 1.4 Hz, 1H, $C_{arom.}$, **6**), 7.12–7.03 (m, 2H, $C_{arom.}$, **iv**/**v**), 6.33 (d, J = 5.5 Hz, 1H, $C_{arom.}$, **d**), 6.23 (d, J = 5.4 Hz, 1H, $C_{arom.}$, **d**), 5.97 (d, J = 5.5 Hz, 1H, $C_{arom.}$, **c**), 5.92 (d, J = 5.4 Hz, 1H, $C_{arom.}$, **c**), 5.30 (ddd, J = 7.8, 1.8, 0.9 Hz, 1H, $C_{arom.}$, **vi**), 2.72 (hept, J = 6.9 Hz, 1H, CH, **f**), 2.34 (s, 3H, CH_3, **a**), 2.20 (dq, J = 12.5, 7.3 Hz, 1H, CH_2, **11**), 2.07 (dq, J = 12.6, 7.3 Hz, 1H, CH_2, **11**), 1.25 (dd, J = 8.3, 6.9 Hz, 6H, CH_3, **g**), 0.76 (t, J = 7.4 Hz, 3H, CH_3, **12**).

^{13}C–NMR (150.9 MHz, DMSO-d6) δ 180.4–180.1 (C_q, **1**/**9**), 135.9 (C_q, **8**), 135.5 (CH, **i**), 134.5 (C_q, **ii**), 133.0 (C_q, **2**), 130.9 (CH, **6**), 130.1 (CH, **4**/**5**), 128.5 (CH, **iv**/**v**), 127.0 (CH, **4**/**5**), 125.7 (CH, **7**), 124.6 (C_q, **vii**), 122.1 (CH, **iv**/**v**), 121.9 (CH, **iii**), 109.6 (CH, **vi**), 109.2 (C_q, **10**), 98.8 (C_q, **3**), 89.0 (C_q, **e**), 87.7 (C_q, **b**), 72.8–72.4 (CH, **d**), 69.1–68.6 (CH, **c**), 31.3 (CH, **f**), 23.1–22.5 (CH_3, **g**), 17.9 (CH_3, **a**), 15.8 (CH_2, **11**), 13.4 (CH_3, **12**).

Solubility: 0.08 mM in PBS (pH 7.4, 1% DMSO).

Elemental analysis: The elemental composition of **1** is shown in Table 5.

Table 5: Elemental Composition of $C_{29}H_{28}N_2O_3Os \cdot 0.25\ H_2O$

	C	H	N	O
Calculated	53.81	4.44	4.33	8.03
Measured	53.86	4.40	4.62	8.22

3.2.4 3-Methylferrocenyl-4-oxo-(1H-*κN*2-pyrazole-1-yl)-(1,4-dihydronaphthalene-1,2-bis(olato)-*κO*1-*κO*2)(η^6-p-cymene)osmium(II) (2)

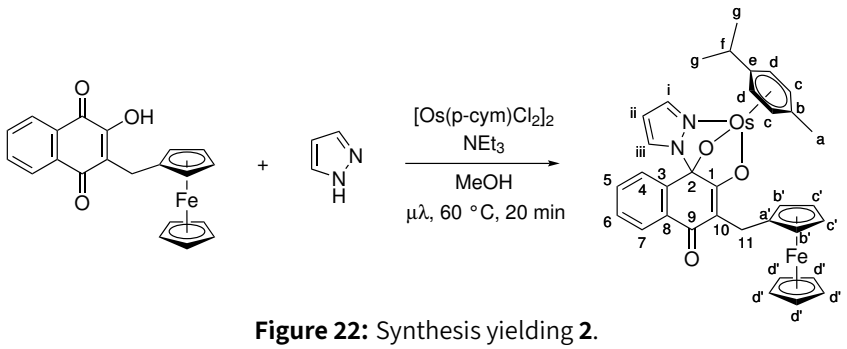

Figure 22: Synthesis yielding **2**.

The synthesis was conducted according to the general procedure, using **IV** (122 mg, 0.154 mmol, 1.00 eq), **II** (109 mg, 0.293 mmol, 1.90 eq), pyrazole (20 mg, 0.29 mmol, 1.9 eq), and NEt_3 (127 µL, 92 mg, 0.91 mmol, 5.9 eq). The pure product was obtained *via* flash chromatography (applied in DCM, 25 g silica, 80% EtOAc/nHex, 5% NEt_3), as a yellow solid (176 mg, 79%).

^{1}H–NMR (600.18 MHz, DMSO-d6) δ 8.42 (dd, J = 2.2, 0.7 Hz, 1H, $C_{arom.}$, **i**), 8.02–7.98 (m, 1H, $C_{arom.}$, **7**), 7.61–7.55 (m, 2H, $C_{arom.}$, **5**/**6**), 7.55–7.49 (m, 1H, $C_{arom.}$, **4**), 6.99 (dd, J = 2.6, 0.7 Hz, 1H, $C_{arom.}$, **iii**), 6.42 (dd, J = 2.4, 2.4 Hz, 1H, $C_{arom.}$, **ii**), 6.22 (dd, J = 43.3, 5.4 Hz, 2H, $C_{arom.}$, **d**), 5.85 (dd, J = 53.2, 5.4 Hz, 2H, $C_{arom.}$, **c**), 3.94 (ddd, J = 2.5, 1.3, 1.3 Hz, 1H, $C_{arom.}$, **b'**/**c'**), 3.92 (s, 5H, $C_{arom.}$, **d'**), 3.86 (ddd, J = 2.3, 2.3, 1.3 Hz, 1H, $C_{arom.}$, **b'**/**c'**), 3.81 (ddd, J = 2.3, 2.3, 1.3 Hz, 1H, $C_{arom.}$, **b'**/**c'**), 3.80–3.77 (m, 1H, $C_{arom.}$, **b'**/**c'**), 3.30 (s, 1H, CH_2, **11**), 3.15 (d, J = 13.9 Hz, 1H, CH_2, **11**), 2.69 (hept, J = 6.9 Hz, 1H, CH, **f**), 2.35 (s, 3H, CH_3, **a**), 1.24 (dd, J = 9.3, 6.9 Hz, 6H, CH_3, **g**).

^{13}C–NMR (150.9 MHz, DMSO-d6) δ 180.4–180.3 (C_q, **1**/**9**), 139.9 (CH, **i**), 135.6–132.6 (C_q, **3**/**8**), 130.8–129.7 (CH, **5**/**6**), 126.3 (CH, **4**), 125.9 (CH, **iii**), 125.6 (CH, **7**), 108.2 (CH, **ii**), 106.9 (C_q, **10**), 98.5 (C_q, **2**), 89.1 (C_q, **a'**), 88.1 (C_q, **e**), 87.2 (C_q, **b**), 72.4 (CH, **d**), 71.7 (CH, **d**), 68.5 (CH, **c**), 68.1,(CH, **c'**) 68.1 (CH, **d'**), 68.0 (CH, **c**), 67.9 (CH, **c'**), 66.0 (CH, **b'**), 65.8 (CH, **b'**), 31.3 (CH, **f**), 23.1 (CH_3, **g**), 22.7 (CH_3, **g**), 22.0 (CH_2, **11**), 18.0 (CH_3, **a**).

Solubility: 0.04 mM in PBS (pH 7.4, 1% DMSO).

Elemental analysis: The elemental composition of **2** is shown in Table 6.

Table 6: Elemental Composition of $C_{34}H_{32}FeN_2O_3Os$

	C	H	N	O
Calculated	53.54	4.23	3.67	6.29
Measured	53.53	4.16	3.73	6.48

3.2.5 3-Methylferrocenyl-4-oxo-(1H-*κN*2-indazole-1-yl)-(1,4-dihydronaphthalene-1,2-bis(olato)-*κO*1-*κO*2)(η^6-p-cymene)osmium(II) (3)

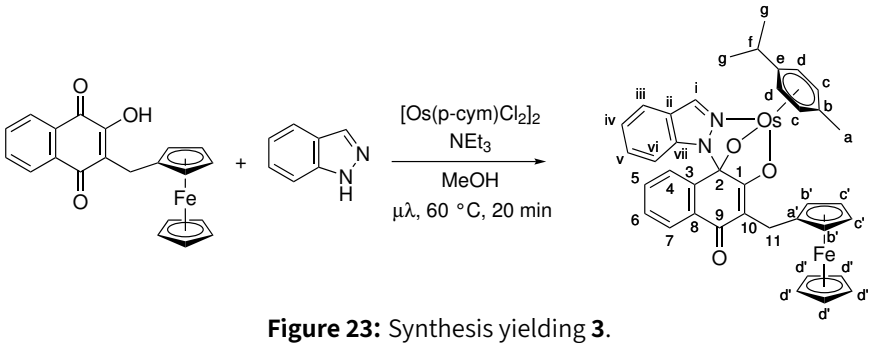

Figure 23: Synthesis yielding **3**.

The synthesis was conducted according to the general procedure, using **IV** (122 mg, 0.154 mmol, 1.00 eq), **II** (109 mg, 0.293 mmol, 1.90 eq), indazole (34 mg, 0.29 mmol, 1.9 eq), and NEt_3 (127 µL, 92 mg, 0.91 mmol, 5.9 eq). The pure product was obtained *via* flash chromatography (applied in DCM, 25 g silica, 80% EtOAc/nHex, 5% NEt_3), as a yellow solid (96 mg, 39%).

^{1}H–NMR (700.40 MHz, DMSO-d6) δ 9.21 (d, J = 0.9 Hz, 1H, $C_{arom.}$, **i**), 8.13 (dd, J = 8.1, 1.4 Hz, 1H, $C_{arom.}$, **7**), 7.87 – 7.81 (m, 1H, $C_{arom.}$, **iii**), 7.69 (m, 2H, $C_{arom.}$, **5**/**6**), 7.62 (ddd, J = 7.3, 7.3, 1.4 Hz, 1H, $C_{arom.}$, **4**), 7.11 (ddd, J = 7.0, 4.7, 3.3 Hz, 2H, $C_{arom.}$, **iv**/**v**), 6.33 (d, J = 5.5 Hz, 1H, $C_{arom.}$, **d**), 6.28 (d, J = 5.4 Hz, 1H, $C_{arom.}$, **d**), 5.99 (d, J = 5.5 Hz, 1H, $C_{arom.}$, **c**), 5.89 (d, J = 5.4 Hz, 1H, $C_{arom.}$, **c**), 5.42 – 5.36 (m, 1H, **vi**), 3.78 (pd, J = 2.4, 1.3 Hz, 2H, $C_{arom.}$, **c'**), 3.71 (ddd, J = 2.3, 2.3, 1.3 Hz, 1H, $C_{arom.}$, **b'**), 3.68 (s, 5H, $C_{arom.}$, **d'**), 3.61 (ddd, J = 2.5, 1.3, 1.3 Hz, 1H, $C_{arom.}$, **b'**), 3.25 (d, J = 14.1 Hz, 1H, CH_2, **11**), 3.09 (d, J = 14.2 Hz, 1H, CH_2, **11**), 2.75 (hept, J = 6.9 Hz, 1H, CH, **f**), 2.38 (s, 3H, CH_3, **a**), 1.27 (dd, J = 8.2, 6.9 Hz, 6H, CH_3, **g**).

^{13}C–NMR (175.9 MHz, DMSO-d6) δ 180.4 (C_q, **9**), 180.3 (C_q, **1**), 135.9 (C_q, **3**), 135.6 (C_q, **i**), 134.6 (C_q, **ii**), 132.9 (C_q, **8**), 131.0 (C_q, **5**), 130.1 (C_q, **6**), 128.6 (CH, **v**), 127.0 (CH, **4**), 125.8 (CH, **7**), 124.7 (C_q, **vii**), 122.2–122.0 (CH, **iii**/**iv**), 109.7 (CH, **vi**), 107.3 (C_q, **10**), 99.0 (C_q, **2**), 89.0–87.6 (C_q, **b**/**e**/**a'**), 73.0–72.3 (CH, **d**), 69.4–68.7 (CH, **c**), 67.9 (CH, **d'**), 67.6–65.6 (CH, **b'**/**c'**), 31.3 (CH, **f**), 23.1–22.7 (CH_3, **g**), 21.9 (CH_2, **11**), 18.0 (CH_3, **a**).

Solubility: 0.05 mM in PBS (pH 7.4, 1% DMSO).

Elemental analysis: The elemental composition of **3** is shown in Table 7.

Table 7: Elemental Composition of $C_{38}H_{34}FeN_2O_3Os$

	C	H	N	O
Calculated	56.16	4.22	3.45	5.91
Measured	56.03	4.15	3.67	6.05

3.2.6 3-Ethy-4-oxo-(2-(2-(2-((1H-*κN*2-indazole-6-yl)oxy)ethoxy)ethoxy)ethan-1-ferrocenylamide)-(1,4-dihydronaphtalene-1,2-bis(olato)-*κO*1-*κO*2)(η^6-p-cymene)osmium(II) (4)

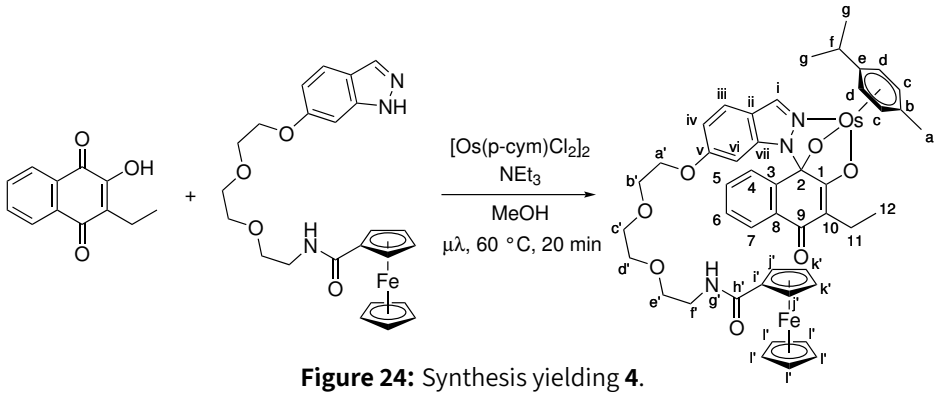

Figure 24: Synthesis yielding **4**.

The synthesis was conducted according to the general procedure, using **IV** (121 mg, 0.153 mmol, 1.00 eq), **I** (58 mg, 0.29 mmol, 1.9 eq), **III** (139 mg, 0.291 mmol, 1.90 eq), and NEt_3 (127 µL, 92 mg, 0.91 mmol, 6.0 eq). The pure product was obtained *via* flash chromatography (applied in mobile phase, 25 g silica, 95% EtOAc/MeOH, 2% concentrated NH_3 solution), as a yellow powder (112 mg, 37%).

^{1}H–NMR (700.40 MHz, DMSO-d6) δ 9.00 (s, 1H, $C_{arom.}$, **i**), 8.13 (ddd, J = 7.3, 1.2, 1.2 Hz, 1H, $C_{arom.}$, **7**), 7.81 (dd, J = 5.8, 5.8 Hz, 1H, NHC=O, **g'**), 7.68–7.67 (m, 3H, $C_{arom.}$, **4**/**6**/**vi**), 7.62 (ddd, J = 7.4, 7.4, 1.4 Hz, 1H, $C_{arom.}$, **5**), 6.73 (dd, J = 9.0, 2.2 Hz, 1H, $C_{arom.}$, **iii**), 6.25 (dd, J = 62.2, 5.5 Hz, 2H, $C_{arom.}$, **d**), 5.92 (dd, J = 33.0, 5.4 Hz, 2H, $C_{arom.}$, **c**), 4.78 (dd, J = 1.9, 1.9 Hz, 2H, $C_{arom.}$, **j'**), 4.54 (d, J = 2.1 Hz, 1H, $C_{arom.}$, **iv**), 4.31 (dd, J = 1.9, 1.9 Hz, 2H, $C_{arom.}$, **k'**), 4.13 (s, 5H, $C_{arom.}$, **l'**), 3.56 – 3.37 (m, 10H, CH_2, **a'**–**e'**), 3.32 (m, 2H, CH_2, **f'**), 2.71 (hept, J = 6.9 Hz, 1H, CH, **f**), 2.35 (s, 3H, CH_3, **a**), 2.26 – 2.05 (m, 2H, CH_2, **11**), 1.25 (dd, J = 8.9, 6.9 Hz, 6H, CH_3, **g**), 0.79 (t, J = 7.4 Hz, 3H, CH_3, **12**).

^{13}C–NMR (176 MHz, DMSO-d6) δ 180.2 (C_q, **1**/**9**), 169.0 (C_q, **h'**), 158.7 (C_q, **v**), 135.9 (C_q, **vii**), 135.6 (C_q, **3**/**8**), 135.2 (CH, **i**), 133.2 (C_q, **3**/**8**), 130.9 (CH, **5**), 130.0 (CH, **4**/**6**), 127.2 (CH, **vi**), 125.6 (CH, **7**), 122.9 (CH, **4**/**6**), 119.3 (C_q, **ii**), 114.7 (CH, **iii**), 109.2 (C_q, **10**), 98.3 (C_q, **2**), 90.9 (CH, **iv**), 88.7 (C_q, **e**), 87.5 (C_q, **b**), 76.5 (C_q, **i'**), 72.7–72.2 (CH, **d**), 69.9 (CH, **k'**), 69.8–69.2 (CH_2, **c'**/**d'**/**e'**), 69.3 (CH, **l'**), 68.9–68.5 (CH, **c**), 68.2 (CH_2, **b'**), 68.1 (CH, **j'**), 66.9 (CH_2, **a'**), 38.7 (CH_2, **f'**), 31.3 (CH, **f**), 23.1–22.5 (CH_3, **g**), 17.9 (CH_3, **a**), 15.8 (CH_2, **11**), 13.4 (CH_3, **12**). **Solubility:** 0.28 mM in PBS (pH 7.4, 1% DMSO).

Elemental analysis: The elemental composition of **4** is shown in Table 8.

Table 8: Elemental Composition of $C_{46}H_{49}FeN_3O_7Os \cdot H_2O$

	C	H	N	O
Calculated	54.17	5.04	4.12	12.55
Measured	53.83	4.83	4.25	12.44

3.2.7 Stability Measurements

Compounds **1**–**4** were dissolved in DMSO to obtain 10 mM stock solutions. To a mixture of 1980 µL PBS buffer (pH 7.4) and 8 µL DMSO was added 12 µL of a stock solution, giving 40 µM dilutions. The samples were immediately measured inside a temperature controlled (21 °C, Peltier Temperature Controller, Julabo AWC 100 recurculating cooler) UV-vis spectrometer (30 min intervals, Perkin Elmer® Lamda 35), using quartz cuvettes. A mixture of 1980 µL PBS buffer and 20 µL DMSO was used as reference.

3.3 Biological Studies

Cytotoxicity, generation of ROS, and cellular accumulation of a compound are examples for properties frequently determined in preclinical studies. In this work MTT assays, DCFH-DA assays, and ICP-MS were utilized to determine these properties in a series of compounds and to give first insight into their anticancer potential.

3.3.1 General Remarks

The cell lines CH1/PA-1 (human ovarian teratocarcinoma, CRC Centre of Cancer Therapeutics, Institute of Cancer Research, Sutton, UK), SW480 (human large intestine adenocarcinoma, American Type Culture Collection, Manassas, VA, USA), A549 (human lung adenocarcinoma, American Type Culture Collection, Manassas, VA, USA), and CT26 (mouse large intestine carcinoma, American Type Culture Collection, Manassas, VA, USA) were used for the conducted experiments. Experiments utilizing CH1/PA-1, SW480, and A549 cells were conducted using Minimum Essential Medium Eagle (EMEM) (Sigma-Aldrich® M2279, Darmstadt, Germany) supplemented with fetal bovine serum (FBS) (10%, SERANA® S-FBS-MX-025, Pessin, Germany), sodium pyruvate solution (1%, Sigma-Aldrich® S8636), non-essential amino acid solution (1%, Sigma-Aldrich® M7145), and L-glutamine (4 mM, Sigma-Aldrich® G7513) as cell culture medium, if not stated otherwise. For CT26 cells, Dulbecco's Modified Eagle's Medium/Nutrient Mixture F-12 Ham (DMEM/F12) (Sigma-Aldrich® D6421) supplemented with FBS (10%, SERANA® S-FBS-MX-025), and L-glutamine (4 mM, Sigma-Aldrich® G7513) was used as cell culture medium. For washing steps, PBS (Sigma-Aldrich® D8537) was used as delivered. Stock solutions were obtained by dissolving compounds in analytical grade DMSO (ThermoFisher D/4120, Kandel, Germany). Cells were incubated at 37 °C and 5% CO_2 atmosphere inside a CO_2 incubator (Binder GmbH, Tuttlingen, Germany). Tissue culture-treated cell culture flasks (75 cm^2, CytoOne® CC7682-4175) and multiwell plates (CytoOne® CC7682-7596, CC7682-7512) were supplied by Starlab International GmbH (Hamburg, Germany) and used as delivered. Cells and solutions were handled inside a biosafety class II cabinet, whenever sterile environment was required.

3.3.2 Subcultivation

Cell culture medium was removed from cell culture flasks and cells were washed with 7 mL of PBS. Cells were detached from their flasks by adding 1.5 mL of trypsin-ethylenediaminetetraacetic acid (EDTA) solution (Sigma-Aldrich® T4049) and incubating them for 1–4 min (CH1/PA-1: 1 min; A549, CT26: 3 min; SW480: 3–4 min). Trypsinization was stopped by the addition of 8.5 mL of medium and complete detachment was verified *via* microscopic inspection. To 15 mL centrifuge tubes were added 7.5–9.7 mL of cell suspension, depending on growth rate and subculturing schedule of the respective cell culture. Cell culture flasks were refilled with medium to a total volume of 12 mL.

Tubes were centrifuged (3 min, 1200 rpm, Megafuge 1.0 R, Heraeus Holding GmbH, Hanau, Germany), supernatant was removed, and pellets were resuspended in 1–8 mL of medium, depending on pellet size. For cell counting, 10 µL of cell suspension was mixed with 90 µL of trypan blue (Sigma-Aldrich® T8154) and the cell density was determined using a Neubauer improved hemocytometer (Paul Marienfeld GmbH & Co. KG, Lauda Königshofen, Germany).

3.3.3 MTT Assay

To the inner 60 wells of a 96-well plate were added 1000 (PA-1), 2000 (SW480, CT26), or 3000 (A549) cells in 100 µL medium per well (Figure 25). The prepared cells were incubated for 24 h, allowing them to resume adherent growth.

Compounds **1**–**8**, **II**, and **III** were dissolved in DMSO and the obtained stock solutions were diluted 1:100 with medium, giving the stock solutions and dilutions shown in Table 9. A dilution series with nine concentrations was obtained by repeatedly diluting samples with medium in 1:2 ratio. Each dilution was added to cells in triplicates with a volume of 100 µL per well, alongside six control wells (cells and medium) and six blanks (medium only), according to Figure 25. The treated cells were incubated for 96 h.

After incubation, all liquid was replaced with 100 µL per well of a 1:6 mixture of MTT solution (12 mM in PBS, ThermoFisher B21187, Kandel, Germany) and Roswell Park Memorial Institute 1640 medium (RPMI 1640) (Sigma-Aldrich® R0883), supplemented with 10% FBS and L-glutamine (4 mM). Following incubation for 4 h, solution was discarded and the precipitated formazan crystals were dissolved in 150 µL DMSO (ThermoFisher D/4120) per well. Formazan solutions were colorimetrically measured using a microplate reader (550 nm, ref. 690 nm, BIO-TEK® ELx808™, Agilent Technologies Inc., Santa Clara, CA, USA).

Table 9: MTT Assay Stock Solutions and Dilutions

	CH1/PA-1		SW480		A549		CT26	
Compound	c_{stock} [mM]	c_{cells} [µM]	c_{stock} [mM]	c_{cells} [µM]	c_{stock} [mM]	c_{cells} [µM]	c_{stock} [mM]	c_{cells} [µM]
1	20.0	100	1.25	6.25	20.0	100	20.0	100
2	10.0	50.0	10.0	50.0	10.0	50.0	1.25	6.25
3	1.25	6.25	5.00	25.0	5.00	25.0	0.625	3.13
4	10.0	50.0	0.625	3.13	10.0	50.0	10.0	50.0
5	20.0	100	0.156	0.781	5.00	25.0	10.0	50.0
6	5.00	25.0	5.00	25.0	5.00	25.0	5.00	25.0
7	1.25	6.25	0.31	1.56	5.00	25.0	0.625	3.13
8	10.0	50.0	0.039	0.195	5.00	25.0	5.00	25.0
II	10.0	50.0	40.0	200	40.0	200	20.0	100
III	20.0	100	20.0	100	20.0	100	10.0	50.0

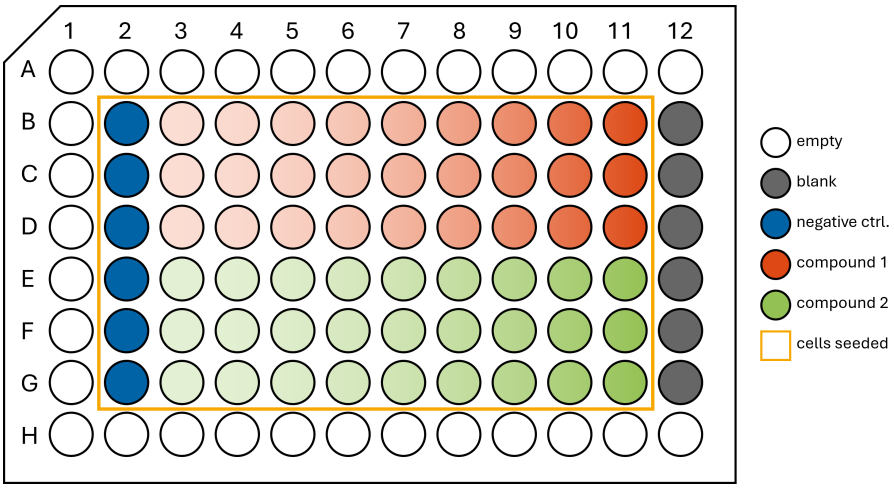

Figure 25: Plate-layout used in MTT assays.

3.3.4 DCFH-DA Assay

Two 96-well plates were prepared by seeding 25,000 cells (SW480) in 100 µL EMEM per well (Figure 26). Cells were incubated for 24 h, allowing them to resume adherent growth.

After incubation, the EMEM was removed from all wells and cells were washed with Hanks' Balanced Salt Solution (HBSS) (Sigma-Aldrich® H6648) supplemented with 1% FBS. A DCFH-DA stock solution (2.5 mM in DMSO, Sigma-Aldrich® D6883) was diluted with HBSS to a final concentration of 25 µM and 100 µL was added per well. Cells were incubated with the DCFH-DA solution for 45 min.

Compound stock solutions were prepared in DMSO with concentrations of 10 (**1**–**5**, **7**, **8**, **II**, **III**) and 5 mM (**6**). The stock solutions were diluted 1:100 with phenol red free OptiMEM® (OptiMEM) (Gibco™ 11058, Fisher Scientific GmbH, Schwerte, Germany) sup-

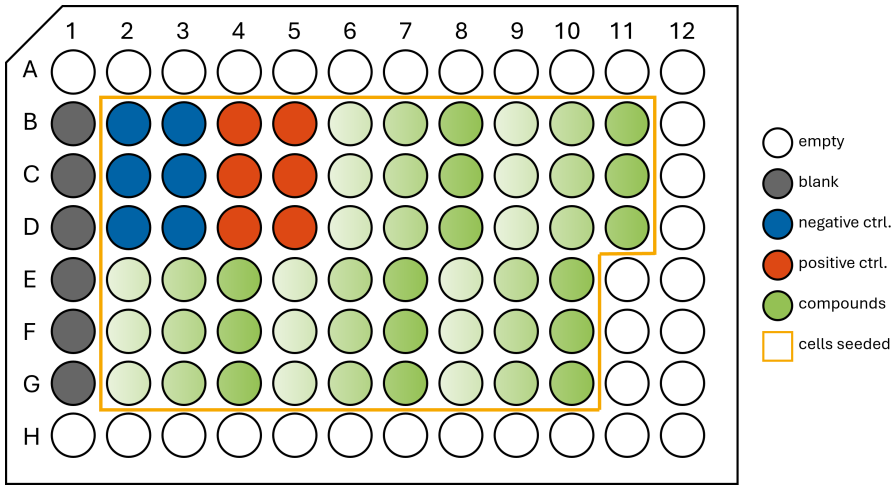

Figure 26: Plate-layout used in DCFH-DA assays.

plemented with 1% FBS. Serial 1:10 dilutions yielded two dilution series with concentrations of 1, 10, and 100 µM; and 0.5, 5, and 50 µM, respectively. For a positive control, a 10 mM tert-butyl hydroperoxide (TBHP) solution was prepared by diluting TBHP (70%, Sigma-Aldrich® 458139) with PBS and further diluting with OptiMEM to concentrations of 200 and 400 µM. The cells were treated according to the scheme in Figure 26, with blanks and negative controls only containing OptiMEM. Fluorescence was measured immediately after application of the substances for a period of 2 h using a BIO-TEK® Synergy™ HT microplate reader (Ex 480, Em 516 nm, 10 min interval).

3.3.5 Cellular Accumulation

Three 12-well plates were seeded with 1,500,000 cells (SW480) per well suspended in 1 mL of EMEM (Figure 27), alongside a reference plate with three comparably seeded wells. Cells were incubated for 24 h.

For compounds **5**–**8**, **II**, and **III**, 1 mM stock solutions were prepared in DMSO. Stocks were diluted with EMEM to a concentration of 5 µM. After incubation, all solution was replaced with 500 µL of the compound solutions (Figure 27), applying every compound to three cell containing wells, as well as three wells without cells. The cells were incubated for 2 h, after which solution was removed from all wells. Every well was washed three times with 1 mL PBS. To each well was added 400 µL of subboiled nitric acid (HNO_3) (69%, Sigma-Aldrich). After 1 h at r.t., 300 µL of solution from each well was transferred to 7.70 mL of MilliQ® water. ^{101}Ru content of the prepared samples was quantified using the ICP-MS 7800 system (Agilent Technologies Inc., CA, USA) equipped with a nickel cone and a SPS4 autosampler (Agilent Technologies Inc.). The ICP was generated using radio-

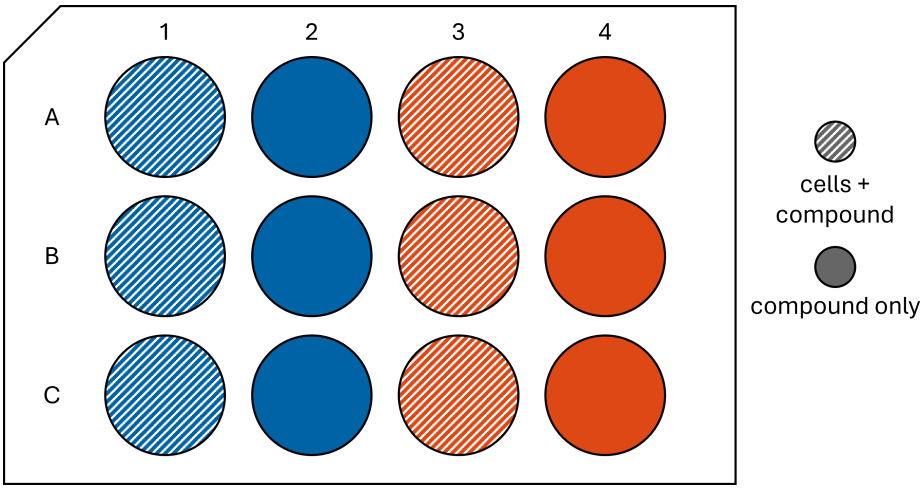

Figure 27: Plate-layout used for cellular accumulation experiments, for two (blue and orange) applied substances.

frequency power of 1.55 kW and carrier- and plasma gas streams of 1.08 and 15 L min^{-1}, respectively. For each sample six replicates were measured in 100 sweeps with an integration time of 0.1 s and evaluated using MassHunter® software (Version C.01.04, Agilent Technologies Inc.). Cell counts were determined for the three reference wells, using a hemocytometer.

4 Conclusion and Outlook

Ruthenium-based piano stool organometallics comprise a promising class of anticancer agents, while osmium derivatives—despite their advantageous properties—have not yet achieved comparable successes. In this work the synthesis of Fc-modified Os complexes was demonstrated and verified using NMR spectroscopy, MS, elemental analysis, and SXRD. Compounds were characterized alongside their Ru analogs, determining stability in aqueous solution, cytotoxicity, capability of inducing ROS, and their cellular accumulation (for Ru complexes only).

Fc-derivatives have been reported to induce ROS *in vitro*.[44–46] Despite successful introduction of Fc into this previously tested class of compounds,[31] cytotoxicity could not be improved. The free ligand **II** exerted significant ROS-induction over the negative control while the Fc-free parent compound was not reported to do so.[31] Fc-containing complexes **2**–**4** and **6**–**8** did not induce ROS, suggesting that ROS do not contribute to the cytotoxicity of the tested complexes.

Despite the apparent lack of ROS-induction, Fc-modified complexes **3**, **4**, and **6**–**8** showed IC_{50} values in the nanomolar range, with **8** exhibiting comparable cytotoxicity to the parent compound.[31] The low IC_{50} of **5** and **8** in SW480 cells was accompanied by greater cellular accumulation. Another trend is the generally lower cytotoxicity of complexes with Fc groups replacing the ethyl groups on the semiquinone chelator, suggesting the importance of this ethyl group for the great biological activity of this compound family in the SW480 cell line.

Although the tested complexes did not induce significant amounts of ROS, the possibilities of introducing Fc as a ROS-inducing group are by no means exhausted. The introduction of Fc *via* an activating group may be a possibility to make Fc groups accessible to redox-cycling, hence allowing for the generation of ROS.

5 References

[1] James Henry Breasted. *The Edwin Smith Surgical Papyrus, Volume 1: Hieroglyphic Transliteration, Translation, and Commentary | Institute for the Study of Ancient Cultures*. 1930. URL: https://isac.uchicago.edu/research/publications/oip/edwin-smith-surgical-papyrus-volume-1-hieroglyphic-transliteration (visited on 06/13/2025).

[2] Hippocrates of Cos. *Aphorisms: Section 6: Aphorism XLVI*. Loeb Classical Library. 1931. URL: https://www.loebclassics.com/view/hippocrates_cos-aphorisms/1931/pb_LCL150.189.xml (visited on 06/09/2025).

[3] Lisa A. Urry et al. *Campbell Biologie*. 12., aktualisierte Auflage. Pearson Studium - Biologie 4451. München: Pearson, 2025. ISBN: 978-3-86894-590-4.

[4] Douglas Hanahan and Robert A. Weinberg. "The Hallmarks of Cancer". In: *Cell* 100.1 (Jan. 7, 2000), pp. 57–70. ISSN: 0092-8674, 1097-4172. DOI: 10.1016/S0092-8674(00)81683-9. PMID: 10647931.

[5] Douglas Hanahan and Robert A. Weinberg. "Hallmarks of Cancer: The Next Generation". In: *Cell* 144.5 (Mar. 2011), pp. 646–674. ISSN: 00928674. DOI: 10.1016/j.cell.2011.02.013.

[6] Douglas Hanahan. "Hallmarks of Cancer: New Dimensions". In: *Cancer Discovery* 12.1 (Jan. 1, 2022), pp. 31–46. ISSN: 2159-8274, 2159-8290. DOI: 10.1158/2159-8290.CD-21-1059.

[7] Wild CP, Weiderpass E, and Stewart BW. *World Cancer Report: Cancer Research for Cancer Prevention*. ISBN: 978-92-832-0447-3 978-92-832-0448-0.

[8] "Global, Regional, and National Comparative Risk Assessment of 84 Behavioural, Environmental and Occupational, and Metabolic Risks or Clusters of Risks for 195 Countries and Territories, 1990–2017: A Systematic Analysis for the Global Burden of Disease Study 2017". In: *Lancet (London, England)* 392.10159 (Nov. 10, 2018), pp. 1923–1994. ISSN: 0140-6736. DOI: 10.1016/S0140-6736(18)32225-6. PMID: 30496105.

[9] J Ferlay et al. *Cancer Today*. Global Cancer Observatory: Cancer Today (version 1.1). 2024. URL: https://gco.iarc.who.int/today/ (visited on 03/02/2026).

[10] Tatiana Tondini, Albert Isidro, and Edgard Camarós. "Case Report: Boundaries of Oncological and Traumatological Medical Care in Ancient Egypt: New Palaeopathological Insights from Two Human Skulls". In: *Frontiers in Medicine* 11 (May 29, 2024), p. 1371645. ISSN: 2296-858X. DOI: 10.3389/fmed.2024.1371645.

[11] Nicholas Eastley, Martyn Newey, and Robert U. Ashford. “Skeletal Metastases – The Role of the Orthopaedic and Spinal Surgeon”. In: *Surgical Oncology* 21.3 (Sept. 1, 2012), pp. 216–222. ISSN: 0960-7404. DOI: 10.1016/j.suronc.2012.04.001.

[12] Samuel M. Meier-Menches et al. “Structure–Activity Relationships for Ruthenium and Osmium Anticancer Agents – towards Clinical Development”. In: *Chemical Society Reviews* 47.3 (2018), pp. 909–928. ISSN: 0306-0012, 1460-4744. DOI: 10.1039/C7CS00332C.

[13] Mikhail V. Blagosklonny. “Analysis of FDA Approved Anticancer Drugs Reveals the Future of Cancer Therapy”. In: *Cell Cycle* 3.8 (Aug. 21, 2004), pp. 1033–1040. ISSN: 1538-4101, 1551-4005. DOI: 10.4161/cc.3.8.1023.

[14] Yeuan Ting Lee, Yi Jer Tan, and Chern Ein Oon. “Molecular Targeted Therapy: Treating Cancer with Specificity”. In: *European Journal of Pharmacology* 834 (Sept. 2018), pp. 188–196. ISSN: 00142999. DOI: 10.1016/j.ejphar.2018.07.034.

[15] Klaus Strebhardt and Axel Ullrich. “Paul Ehrlich’s Magic Bullet Concept: 100 Years of Progress”. In: *Nature Reviews Cancer* 8.6 (June 2008), pp. 473–480. ISSN: 1474-175X, 1474-1768. DOI: 10.1038/nrc2394.

[16] Malay Patra and Gilles Gasser. “The Medicinal Chemistry of Ferrocene and Its Derivatives”. In: *Nature Reviews Chemistry* 1.9 (Sept. 6, 2017), p. 0066. ISSN: 2397-3358. DOI: 10.1038/s41570-017-0066.

[17] Sofia Farkona, Eleftherios P. Diamandis, and Ivan M. Blasutig. “Cancer Immunotherapy: The Beginning of the End of Cancer?” In: *BMC Medicine* 14.1 (Dec. 2016), p. 73. ISSN: 1741-7015. DOI: 10.1186/s12916-016-0623-5.

[18] Dinh-Toi Chu et al. “Recent Progress of Stem Cell Therapy in Cancer Treatment: Molecular Mechanisms and Potential Applications”. In: *Cells* 9.3 (Mar. 2020), p. 563. ISSN: 2073-4409. DOI: 10.3390/cells9030563.

[19] M. Peyrone. “Ueber die Einwirkung von Ammoniak auf Platinchlorür”. In: *Justus Liebigs Annalen der Chemie* 55.2 (Jan. 1845), pp. 205–213. ISSN: 0075-4617. DOI: 10.1002/jlac.18450550206.

[20] Barnett Rosenberg, Loretta Van Camp, and Thomas Krigas. “Inhibition of Cell Division in Escherichia Coli by Electrolysis Products from a Platinum Electrode”. In: *Nature* 205.4972 (Feb. 1965), pp. 698–699. ISSN: 1476-4687. DOI: 10.1038/205698a0.

[21] Barnett Rosenberg et al. “Platinum Compounds: A New Class of Potent Antitumour Agents”. In: *Nature* 222.5191 (Apr. 1969), pp. 385–386. ISSN: 1476-4687. DOI: 10.1038/222385a0.

[22] L Galluzzi et al. “Molecular Mechanisms of Cisplatin Resistance”. In: *Oncogene* 31.15 (Apr. 12, 2012), pp. 1869–1883. ISSN: 0950-9232, 1476-5594. DOI: 10.1038/onc.2011.384.

[23] David McAlpine and Brian M. Johnstone. “The Ototoxic Mechanism of Cisplatin”. In: *Hearing Research* 47.3 (Aug. 1990), pp. 191–203. ISSN: 03785955. DOI: 10.1016/0378-5955(90)90151-E.

[24] Shaloam Dasari and Paul Bernard Tchounwou. “Cisplatin in Cancer Therapy: Molecular Mechanisms of Action”. In: *European Journal of Pharmacology* 740 (Oct. 2014), pp. 364–378. ISSN: 00142999. DOI: 10.1016/j.ejphar.2014.07.025.

[25] Paul D. O’Dowd, Darragh F. Sutcliffe, and Darren M. Griffith. “Oxaliplatin and Its Derivatives – An Overview”. In: *Coordination Chemistry Reviews* 497 (Dec. 2023), p. 215439. ISSN: 00108545. DOI: 10.1016/j.ccr.2023.215439.

[26] Peter M. Bruno et al. “A Subset of Platinum-Containing Chemotherapeutic Agents Kills Cells by Inducing Ribosome Biogenesis Stress”. In: *Nature Medicine* 23.4 (Apr. 2017), pp. 461–471. ISSN: 1546-170X. DOI: 10.1038/nm.4291.

[27] Benjamin Neuditschko et al. “Interaction with Ribosomal Proteins Accompanies Stress Induction of the Anticancer Metallodrug BOLD-100/KP1339 in the Endoplasmic Reticulum”. In: *Angewandte Chemie International Edition* 60.10 (2021), pp. 5063–5068. ISSN: 1521-3773. DOI: 10.1002/anie.202015962.

[28] Jenifer B. Gifford et al. “Expression of GRP78, Master Regulator of the Unfolded Protein Response, Increases Chemoresistance in Pancreatic Ductal Adenocarcinoma”. In: *Molecular Cancer Therapeutics* 15.5 (May 2016), pp. 1043–1052. ISSN: 1538-8514. DOI: 10.1158/1535-7163.MCT-15-0774. PMID: 26939701.

[29] Susan Monro et al. “Transition Metal Complexes and Photodynamic Therapy from a Tumor-Centered Approach: Challenges, Opportunities, and Highlights from the Development of TLD1433”. In: *Chemical Reviews* 119.2 (Jan. 23, 2019), pp. 797–828. ISSN: 0009-2665. DOI: 10.1021/acs.chemrev.8b00211.

[30] Benjamin S. Murray et al. “The Development of RAPTA Compounds for the Treatment of Tumors”. In: *Coordination Chemistry Reviews* 306 (Jan. 1, 2016), pp. 86–114. ISSN: 0010-8545. DOI: 10.1016/j.ccr.2015.06.014.

[31] Heiko Geisler et al. “Tridentate 3-Substituted Naphthoquinone Ruthenium Arene Complexes: Synthesis, Characterization, Aqueous Behavior, and Theoretical and Biological Studies”. In: *Inorganic Chemistry* 60.13 (July 5, 2021), pp. 9805–9819. ISSN: 0020-1669, 1520-510X. DOI: 10.1021/acs.inorgchem.1c01083.

[32] Alexander Rosner et al. “Selectivity for TP53 Signalling Drives the Mode of Action of a Highly Potent N , O , O -Tridentate Naphthoquinone-Based Organo-Ruthenium Anticancer Drug Candidate”. In: *Chemical Science* 16.34 (2025), pp. 15652–15665. DOI: 10.1039/D5SC00735F.

[33] John W. Howell. “Metal Filament Lamps”. In: *Proceedings of the American Institute of Electrical Engineers* 29.6 (June 1910), pp. 819–830. ISSN: 2376-7758. DOI: 10.1109/PAIEE.1910.6660123.

[34] Robert W. Cumberland et al. “Osmium Diboride, An Ultra-Incompressible, Hard Material”. In: *Journal of the American Chemical Society* 127.20 (May 25, 2005), pp. 7264–7265. ISSN: 0002-7863. DOI: 10.1021/ja043806y.

[35] Brenden Carlson et al. “Divalent Osmium Complexes: Synthesis, Characterization, Strong Red Phosphorescence, and Electrophosphorescence”. In: *Journal of the American Chemical Society* 124.47 (Nov. 1, 2002), pp. 14162–14172. ISSN: 0002-7863, 1520-5126. DOI: 10.1021/ja0176705.

[36] Giorgio Chelucci, Salvatore Baldino, and Walter Baratta. “Recent Advances in Osmium-Catalyzed Hydrogenation and Dehydrogenation Reactions”. In: *Accounts of Chemical Research* 48.2 (Feb. 17, 2015), pp. 363–379. ISSN: 0001-4842. DOI: 10.1021/ar5003818.

[37] Vincent Brian Wigglesworth. “The Use of Osmium in the Fixation and Staining of Tissues”. In: *Proceedings of the Royal Society of London. B. Biological Sciences* 147.927 (Sept. 12, 1957), pp. 185–199. ISSN: 0080-4649. DOI: 10.1098/rspb.1957.0043.

[38] Antoine Dorcier et al. “In Vitro Evaluation of Rhodium and Osmium RAPTA Analogues: The Case for Organometallic Anticancer Drugs Not Based on Ruthenium”. In: *Organometallics* 25.17 (Aug. 1, 2006), pp. 4090–4096. ISSN: 0276-7333. DOI: 10.1021/om060394o.

[39] Berta Cebrián-Losantos et al. “Osmium NAMI-A Analogues: Synthesis, Structural and Spectroscopic Characterization, and Antiproliferative Properties”. In: *Inorganic Chemistry* 46.12 (June 1, 2007), pp. 5023–5033. ISSN: 0020-1669. DOI: 10.1021/ic700405y.

[40] Gabriel E. Büchel et al. “En Route to Osmium Analogues of KP1019: Synthesis, Structure, Spectroscopic Properties and Antiproliferative Activity of Trans-[OsIVCl4(Hazole)2]”. In: *Inorganic Chemistry* 50.16 (Aug. 15, 2011), pp. 7690–7697. ISSN: 0020-1669. DOI: 10.1021/ic200728b. PMID: 21739939.

[41] Muhammad Hanif, Maria V. Babak, and Christian G. Hartinger. “Development of Anticancer Agents: Wizardry with Osmium”. In: *Drug Discovery Today* 19.10 (Oct. 2014), pp. 1640–1648. ISSN: 13596446. DOI: 10.1016/j.drudis.2014.06.016.

[42] Wen-Xiu Ni et al. “Osmium(VI) Nitrido Complexes Bearing Azole Heterocycles: A New Class of Antitumor Agents”. In: *Chemical Science* 3.5 (Apr. 2, 2012), pp. 1582–1588. ISSN: 2041-6539. DOI: 10.1039/C2SC01031C.

[43] T. J. Kealy and P. L. Pauson. “A New Type of Organo-Iron Compound”. In: *Nature* 168.4285 (Dec. 1951), pp. 1039–1040. ISSN: 1476-4687. DOI: 10.1038/1681039b0.

[44] Giovanni Tabbì et al. “Water Stability and Cytotoxic Activity Relationship of a Series of Ferrocenium Derivatives. ESR Insights on the Radical Production during the Degradation Process”. In: *Journal of Medicinal Chemistry* 45.26 (Dec. 1, 2002), pp. 5786–5796. ISSN: 0022-2623, 1520-4804. DOI: 10.1021/jm021003k.

[45] Faustine Dubar et al. “The Antimalarial Ferroquine: Role of the Metal and Intramolecular Hydrogen Bond in Activity and Resistance”. In: *ACS Chemical Biology* 6.3 (Mar. 18, 2011), pp. 275–287. ISSN: 1554-8929, 1554-8937. DOI: 10.1021/cb100322v.

[46] Domenico Osella et al. “On the Mechanism of the Antitumor Activity of Ferrocenium Derivatives”. In: *Inorganica Chimica Acta* 306.1 (Aug. 2000), pp. 42–48. ISSN: 00201693. DOI: 10.1016/S0020-1693(00)00147-X.

[47] Karin Schlotter et al. “Fancy Bioisosteres: Metallocene-Derived G-Protein-Coupled Receptor Ligands with Subnanomolar Binding Affinity and Novel Selectivity Profiles”. In: *Journal of Medicinal Chemistry* 48.11 (June 1, 2005), pp. 3696–3699. ISSN: 0022-2623, 1520-4804. DOI: 10.1021/jm050170s.

[48] Koushambi Mitra et al. “Remarkable Anticancer Activity of Ferrocenyl-Terpyridine Platinum(Ii) Complexes in Visible Light with Low Dark Toxicity”. In: (Dec. 4, 2013). DOI: 10.1039/C3DT51922H.

[49] Carlo M. Bergamini et al. “Oxygen, Reactive Oxygen Species and Tissue Damage”. In: *Current Pharmaceutical Design* 10.14 (May 1, 2004), pp. 1611–1626. DOI: 10.2174/1381612043384664.

[50] H. J. H. Fenton. “LXXIII.—Oxidation of Tartaric Acid in Presence of Iron”. In: *Journal of the Chemical Society, Transactions* 65.0 (Jan. 1, 1894), pp. 899–910. ISSN: 0368-1645. DOI: 10.1039/CT8946500899.

[51] Robert A. Greenwald. *Handbook Methods For Oxygen Radical Research*. CRC Press, Feb. 1, 2018. 468 pp. ISBN: 978-1-351-08137-5. Google Books: tixKDwAAQBAJ.

[52] Victor M. Samokyszyn et al. “Release of Iron from Ferritin and Its Role in Oxygen Radical Toxicities”. In: *Drug Metabolism Reviews* 19.3–4 (Jan. 1988), pp. 283–303. ISSN: 0360-2532, 1097-9883. DOI: 10.3109/03602538808994137.

[53] George O. Gey, Ward D. Coffman, and Mary T. Kubicek. “Tissue Culture Studies of the Proliferative Capacity of Cervical Carcinoma and Normal Epithelium.” In: *Cancer Research* 12.4 (Apr. 1952), pp. 264–265.

[54] Bruce A. Ruggeri, Faye Camp, and Sheila Miknyoczki. “Animal Models of Disease: Pre-clinical Animal Models of Cancer and Their Applications and Utility in Drug Discovery”. In: *Biochemical Pharmacology* 87.1 (Jan. 2014), pp. 150–161. ISSN: 00062952. DOI: 10.1016/j.bcp.2013.06.020.

[55] Rashi Rai et al. “Cancer: Clinical Trial Design and Principles”. In: *Advances in Medical Diagnosis, Treatment, and Care*. Ed. by Sumit Kumar, Moshahid Alam Rizvi, and Saurabh Verma. IGI Global, 2021, pp. 627–638. ISBN: 978-1-7998-6530-8 978-1-7998-6531-5. DOI: 10.4018/978-1-7998-6530-8.ch024.

[56] Tim Mosmann. “Rapid Colorimetric Assay for Cellular Growth and Survival: Application to Proliferation and Cytotoxicity Assays”. In: *Journal of Immunological Methods* 65.1–2 (Dec. 1983), pp. 55–63. ISSN: 00221759. DOI: 10.1016/0022-1759(83)90303-4.

[57] Rossella Marullo et al. “Cisplatin Induces a Mitochondrial-ROS Response That Contributes to Cytotoxicity Depending on Mitochondrial Redox Status and Bioenergetic Functions”. In: *PLoS ONE* 8.11 (Nov. 19, 2013). Ed. by Robert W Sobol, e81162. ISSN: 1932-6203. DOI: 10.1371/journal.pone.0081162.

[58] Albert S. Keston and Richard Brandt. “The Fluorometric Analysis of Ultramicro Quantities of Hydrogen Peroxide”. In: *Analytical Biochemistry* 11.1 (Apr. 1, 1965), pp. 1–5. ISSN: 0003-2697. DOI: 10.1016/0003-2697(65)90034-5.

[59] Richard Brandt and Albert S. Keston. “Synthesis of Diacetyldichlorofluorescin: A Stable Reagent for Fluorometric Analysis”. In: *Analytical Biochemistry* 11.1 (Apr. 1, 1965), pp. 6–9. ISSN: 0003-2697. DOI: 10.1016/0003-2697(65)90035-7.

[60] D. J. Douglas, E. S. K. Quan, and R. G. Smith. “Elemental Analysis with an Atmospheric Pressure Plasma (MIP, ICP)/Quadrupole Mass Spectrometer System”. In: *Spectrochimica Acta Part B: Atomic Spectroscopy* 38.1 (Jan. 1, 1983), pp. 39–48. ISSN: 0584-8547. DOI: 10.1016/0584-8547(83)80101-3.

[61] Bruno Therrien, Adrian König, and Thomas R. Ward. “Synthesis of a Configurationally Stable Three-Legged Piano-Stool Complex”. In: *Organometallics* 18.8 (Apr. 1, 1999), pp. 1565–1568. ISSN: 0276-7333, 1520-6041. DOI: 10.1021/om980949i.

[62] Patrycja Rogala et al. “Synthesis, Crystal Structure and Cytotoxic Activity of Ruthenium(II) Piano-Stool Complex with N,N-chelating Ligand”. In: *Journal of Molecular Structure* 1126 (Dec. 2016), pp. 74–82. ISSN: 00222860. DOI: 10.1016/j.molstruc.2016.01.079.

6 Appendix

6.1 NMR Spectra

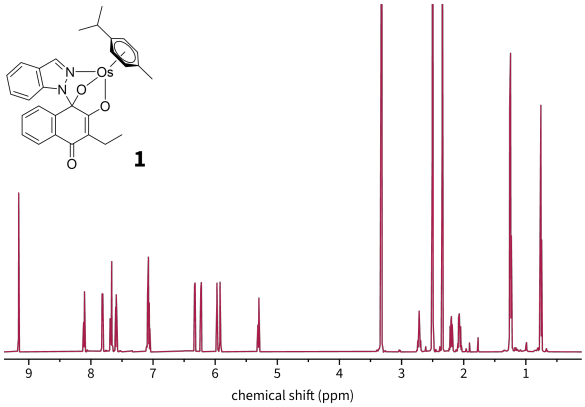

Figure 28: ^{1}H–NMR spectrum of **1**.

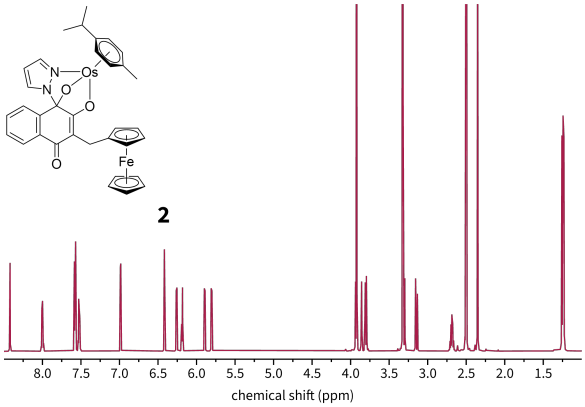

Figure 29: ^{1}H–NMR spectrum of **2**.

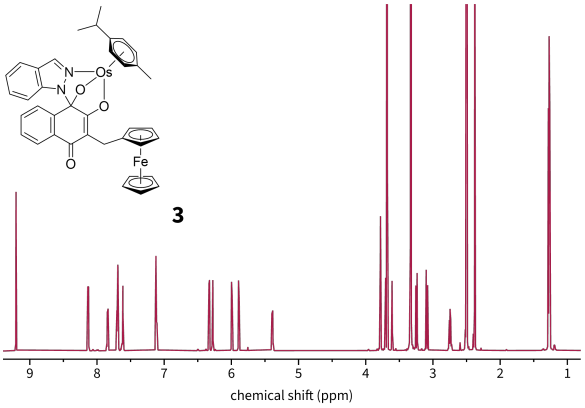

Figure 30: ^{1}H–NMR spectrum of **3**.

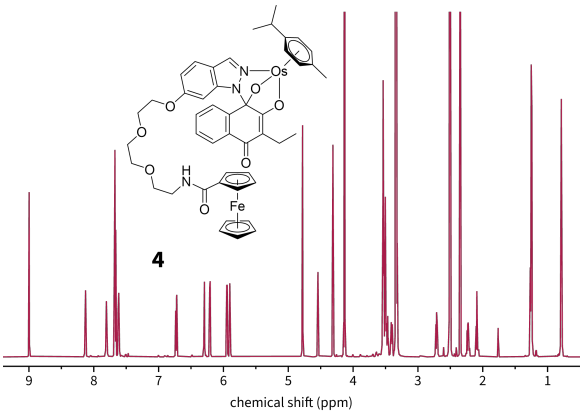

Figure 31: ^{1}H–NMR spectrum of **4**.

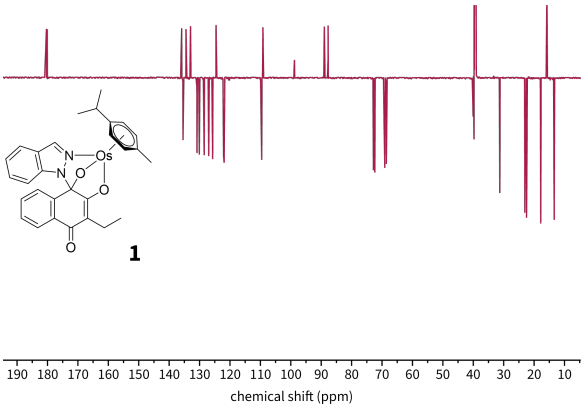

Figure 32: ^{13}C–NMR spectrum of **1**.

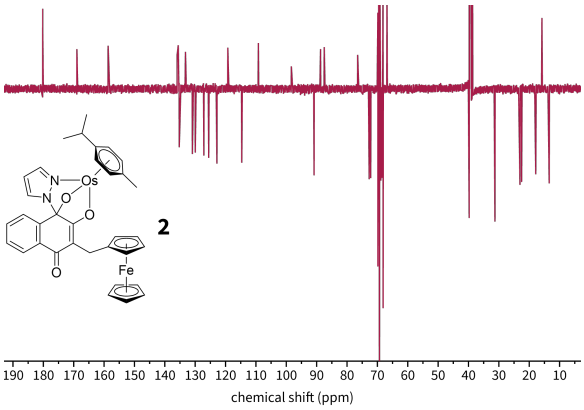

Figure 33: ^{13}C–NMR spectrum of **2**.

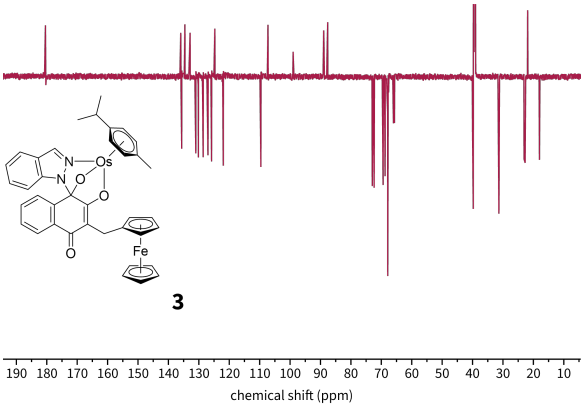

Figure 34: ^{13}C–NMR spectrum of **3**.

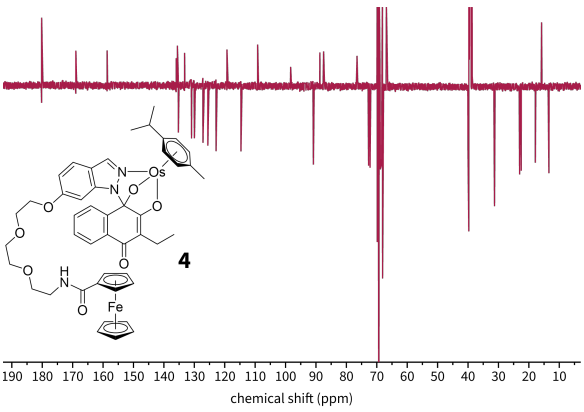

Figure 35: ^{13}C–NMR spectrum of **4**.

6.2 Mass Spectra

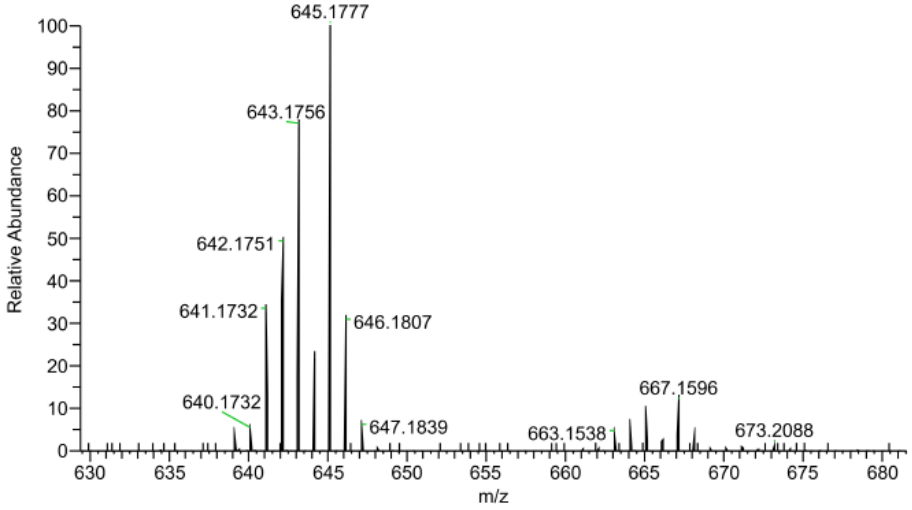

Figure 36: Mass spectrum of **1**.

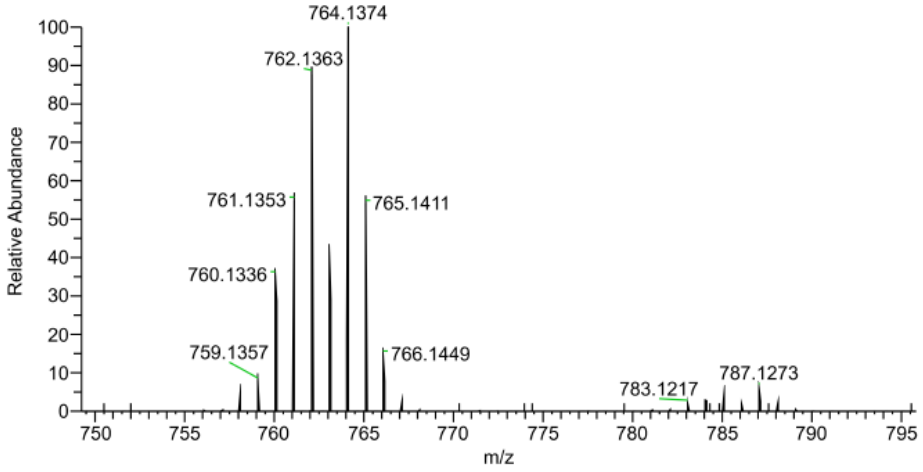

Figure 37: Mass spectrum of **2**.

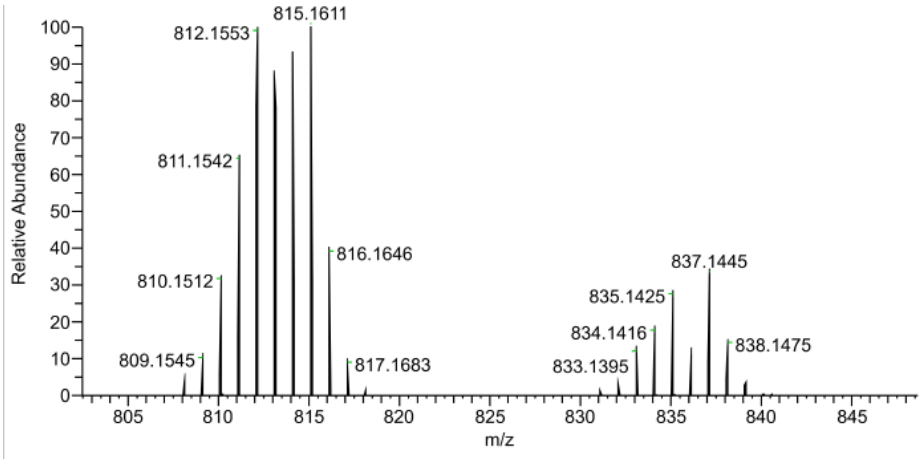

Figure 38: Mass spectrum of **3**.

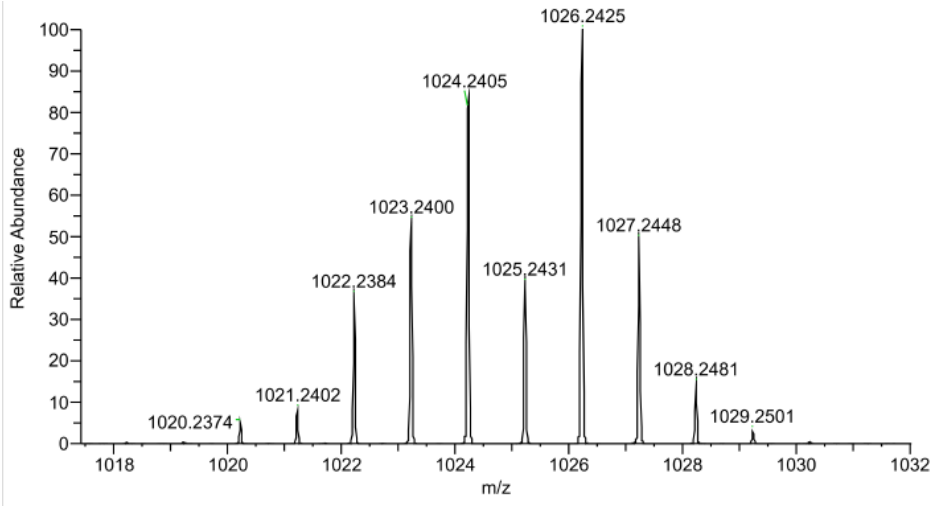

Figure 39: Mass spectrum of **4**.

6.3 Concentration-Effect Curves

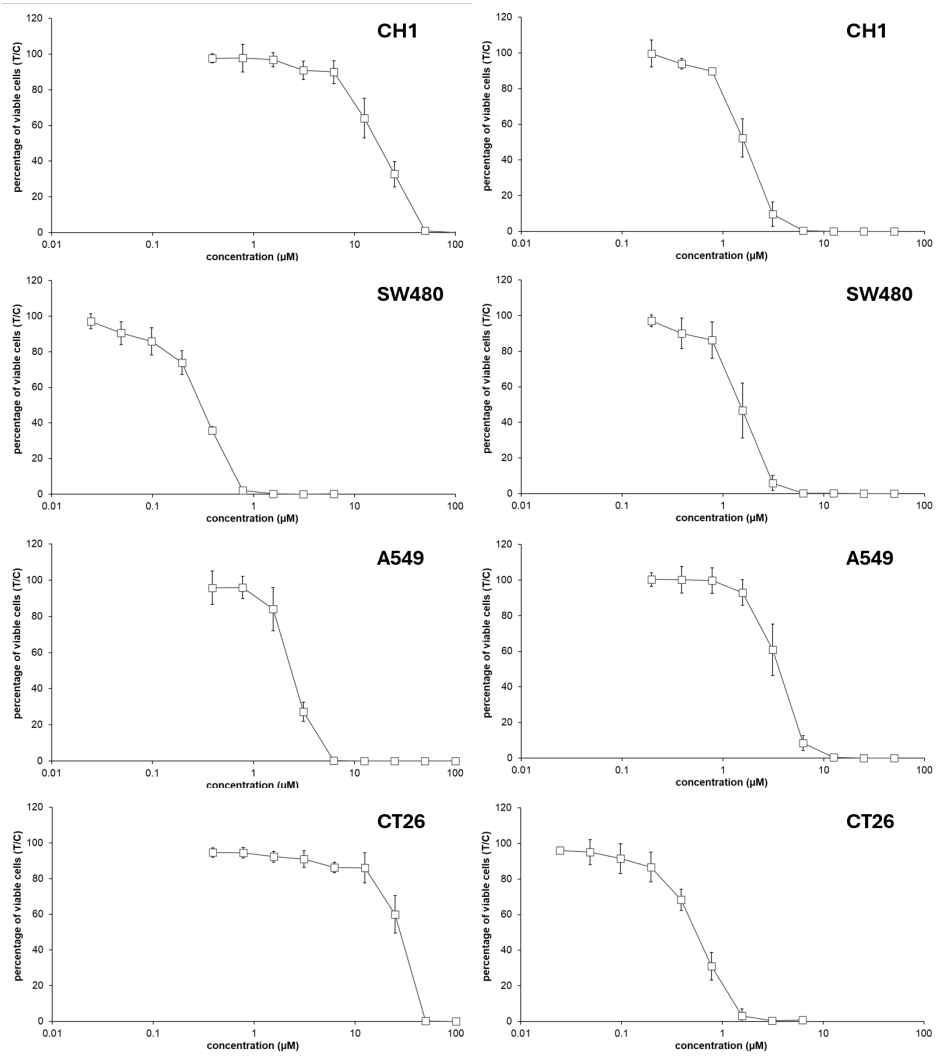

Figure 40: Concentration-effect curves of **1** (left) and **2** (right) in the cell lines CH1/PA-1, SW480, A549, and CT26.

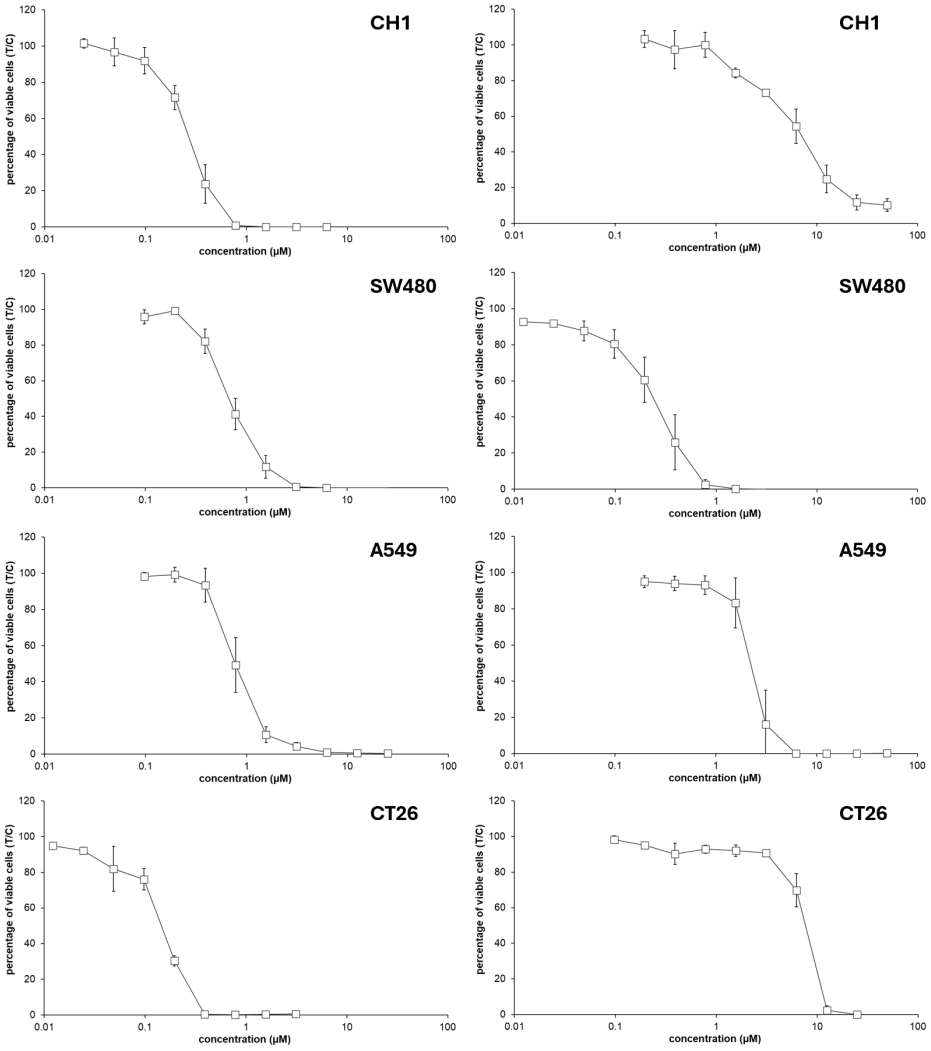

Figure 41: Concentration-effect curves of **3** (left) and **4** (right) in the cell lines CH1/PA-1, SW480, A549, and CT26.

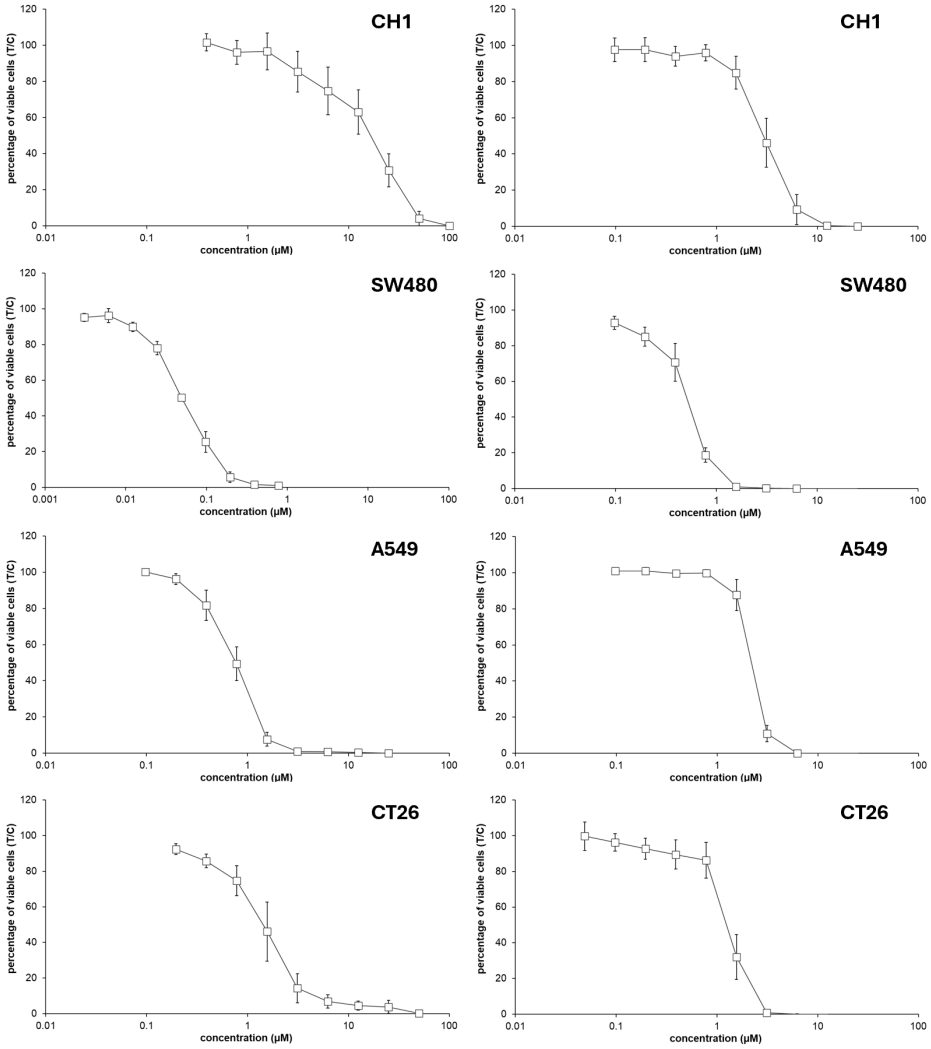

Figure 42: Concentration-effect curves of **5** (left) and **6** (right) in the cell lines CH1/PA-1, SW480, A549, and CT26.

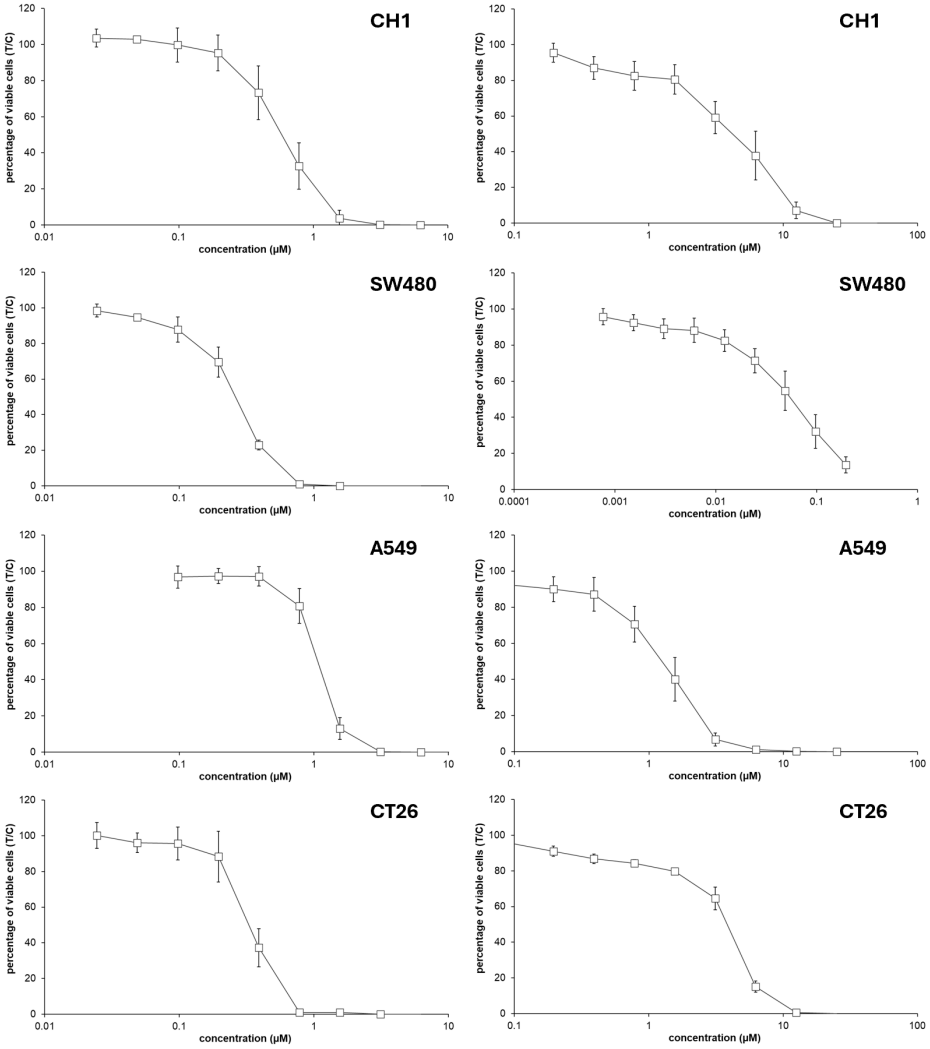

Figure 43: Concentration-effect curves of **7** (left) and **8** (right) in the cell lines CH1/PA-1, SW480, A549, and CT26.

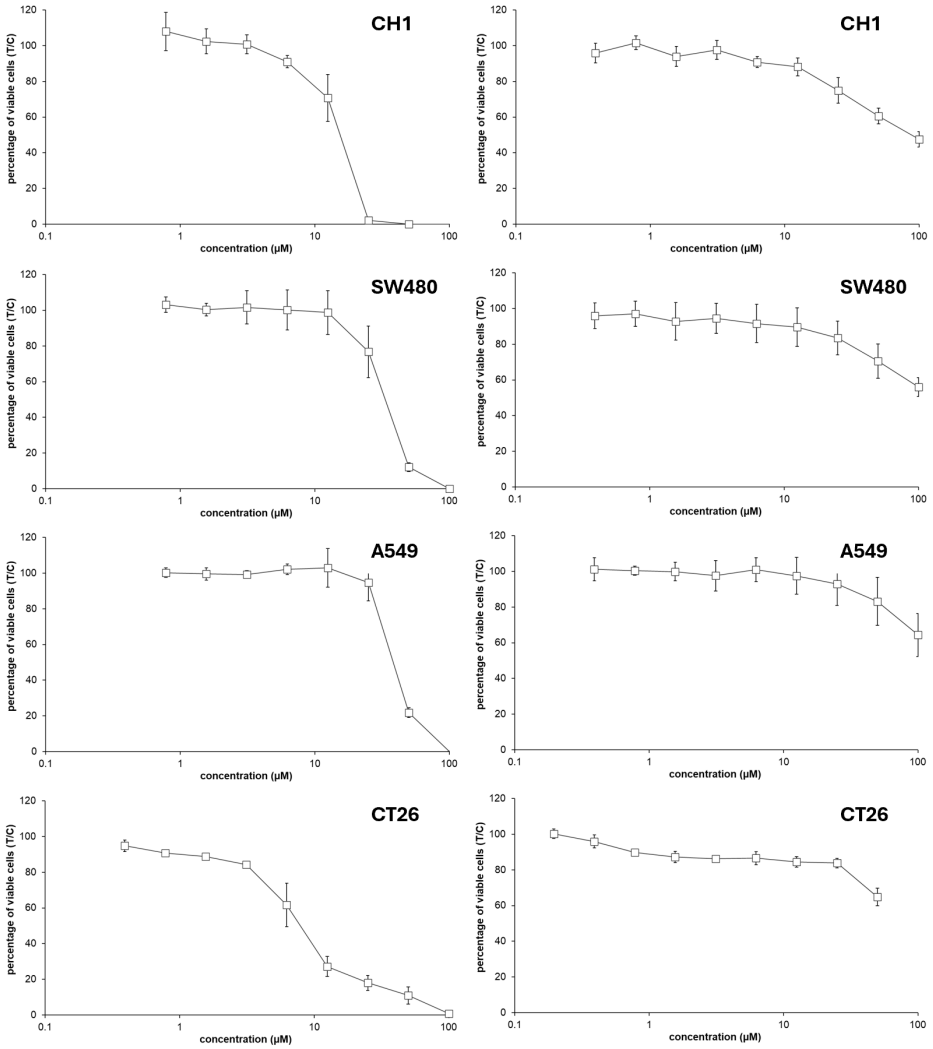

Figure 44: Concentration-effect curves of **II** (left) and **III** (right) in the cell lines CH1/PA-1, SW480, A549, and CT26.

6.4 DCFH-DA Curves

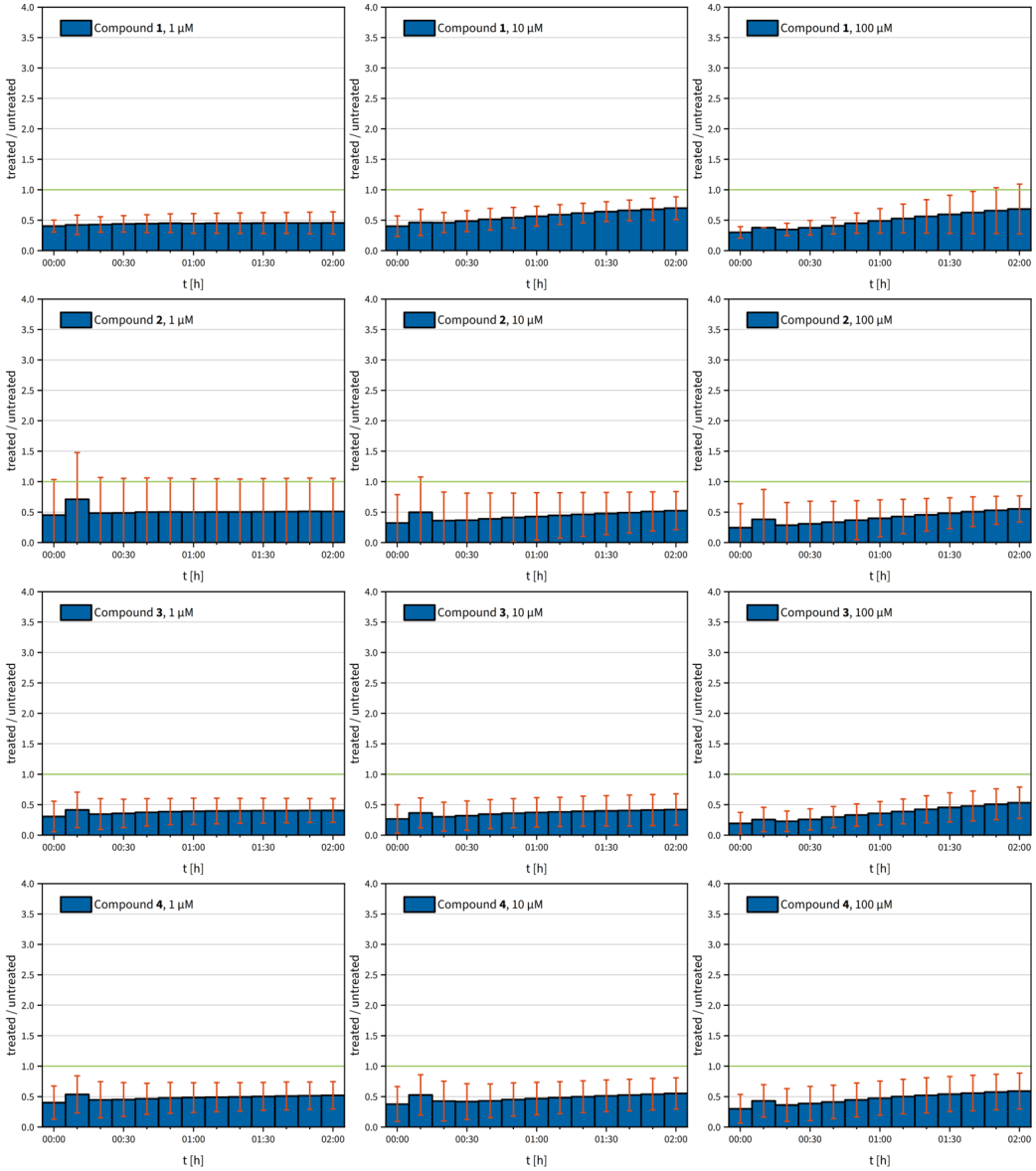

Figure 45: Fluorescent intensities of **1**, **2**, **3**, and **4** over 2 h relative to the negative control.

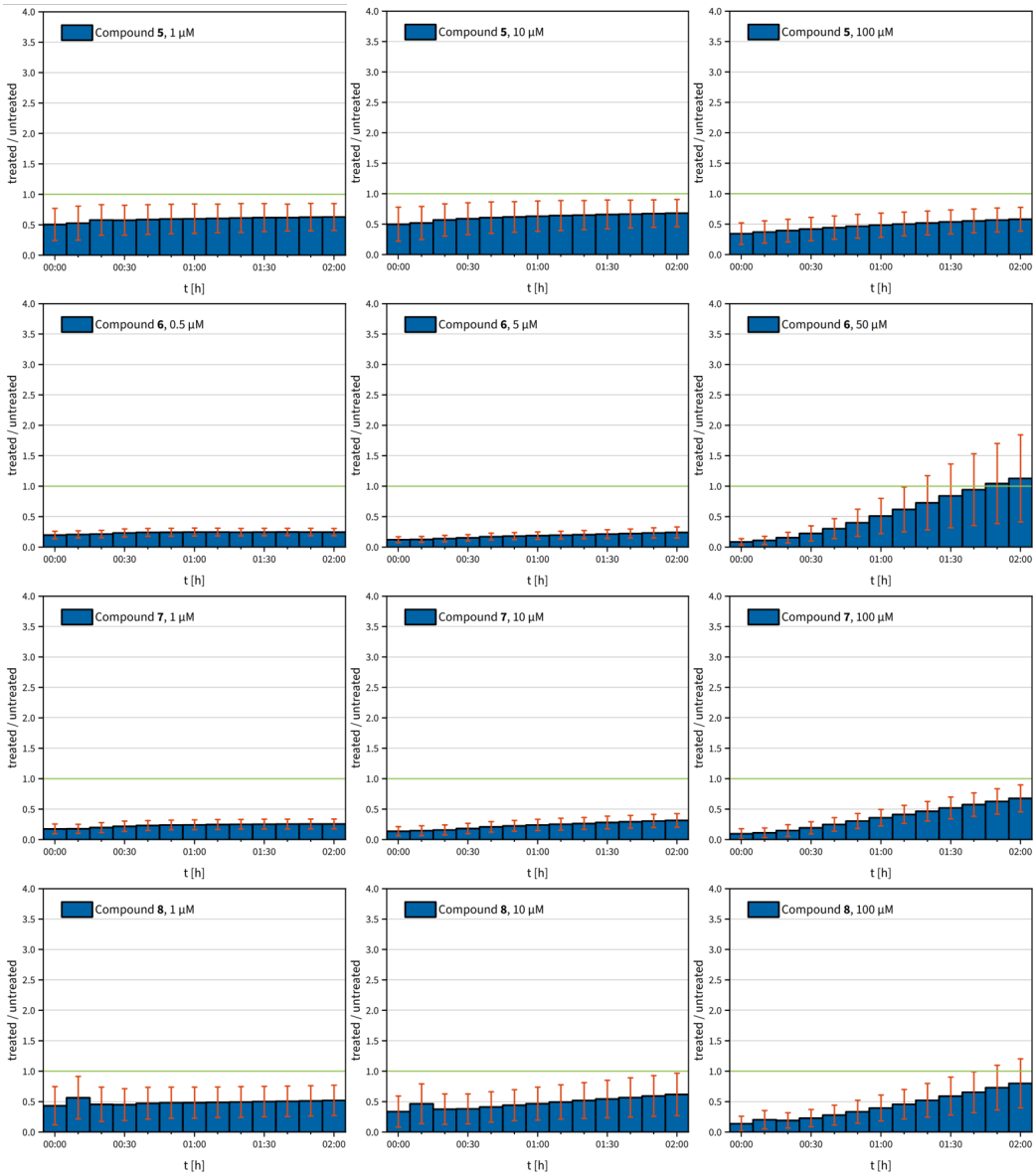

Figure 46: Fluorescent intensities of **5**, **6**, **7**, and **8** over 2 h relative to the negative control.

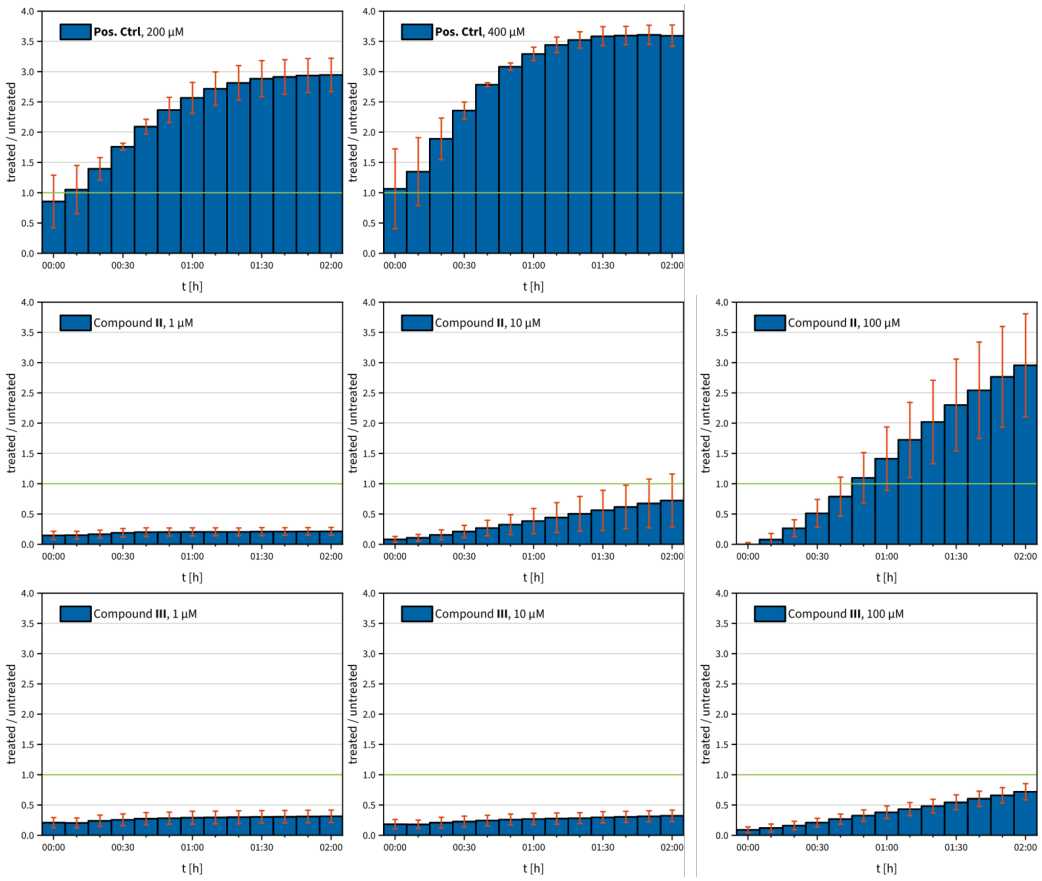

Figure 47: Fluorescent intensities of **II**, **III**, and a TBHP positive control over 2 h relative to the negative control.